Review

Kinetics for Catalytic Pyrolysis of Organic Solid Wastes

Shri Ram [1], Yogesh Patil [2], Fatma Abdelrhman [1,3], Tarique Ahmed Memon [4], and Yaning Zhang [1,*]

[1] School of Energy Science and Engineering, Harbin Institute of Technology, Harbin 150001, China
[2] College of Biosystems Engineering and Food Science, Zhejiang University, Hangzhou 310058, China
[3] Agricultural Engineering Department, Faculty of Agriculture, Cairo University, Giza 12613, Egypt
[4] Department of Mechanical Engineering, The University of Larkano, Larkana 77150, Pakistan
* Correspondence: ynzhang@hit.edu.cn; Tel.: +86-451-86412078
Received: 24 November 2025; Revised: 26 December 2025; Accepted: 26 December 2025; Published: 30 December 2025

Abstract: Catalytic pyrolysis has emerged as a pivotal technology for converting renewable diverse feedstocks (i.e., lignocellulosic biomass, algal biomass, and plastic wastes) into biofuels and chemicals. This review comprehensively examines the reaction kinetics in catalytic pyrolysis, addressing the fundamental gap between lab-scale research and industrial applications. The mechanisms of conventional (i.e., electrical heating) and microwave-assisted catalytic pyrolysis are detailed, highlighting the role of catalysts in altering reaction rates, reaction pathways, and decreasing activation energies. This paper delves into kinetic analysis techniques by comparing the model-free and model-fitting approaches and exploring the emerging role of machine learning in predicting kinetic parameters. In addition, it extensively explores the feedstock specific kinetic models, highlighting the behavior of pseudo-components of lignocellulosic feedstocks, plastic wastes, and their mixtures with a specific focus on synergistic effect during co-pyrolysis. Further, an essential framework to integrate molecular-scale phenomena with reactor-scale process performance was presented by exploring the advanced modelling techniques such as microkinetic modelling using density functional theory (DFT), lumped system analysis using process simulations, and catalyst deactivation kinetics. Despite its promise, challenges such as catalyst deactivation, heat and mass transfer limitations, and feedstock variability remain critical hurdles. This review concludes by identifying future research directions, emphasizing the in-situ characterization, integration of machine learning and artificial intelligence for process optimization, and kinetics of emerging catalyst systems to facilitate the commercial deployment of predictive models for catalytic pyrolysis technologies.

Keywords: pyrolysis; catalyst; kinetics; plastic waste; biomass

1. Introduction

Increasing global waste crisis demands sustainable and innovative management strategies, as traditional methods are insufficient for waste disposal [1,2]. The global waste crisis is determined by generation of massive mounting bulks of municipal, domestic, agricultural and industrial wastes. The larger part of these wastes is generated through rapid industrialization and population growth, resulting into enhanced municipal solid waste (MSW) generation through consumption of goods and materials [3,4]. This trend also drives greater exploitation of fossil fuels, accelerating climate change through greenhouse gas emissions [5]. At the same time, waste plastics have also created severe environmental pollutions, posing threats to ecosystem [6]. It presents a critical challenge for sustainable environment and indicates towards growing need of recycling and upcycling of wastes [7]. However, the sustainable carbon materials produced from renewable and waste resources have shown a good potential in environmental remediation and energy conversion systems [8]. In addition, the conversion of waste to useful energy forms has emerged as a promising solution to produce renewable energy [9].

Diverse biomass feedstocks are recognized for their renewability, accessibility, and carbon-neutrality [10,11]. In the present times, 80% of the energy demands are fulfilled with the help of fossil fuels, but the biomass which has abundancy (100 billion tons per annum) can be used in energy mix to reduce over-dependence over fossil fuels. The biomass utilization has been directed and accelerated in current times after the EU's Renewable Energy Directive and U.S. Bioeconomy Initiative with biomass to fulfil around 20–30% of total renewable energy production by 2030 [12,13]. Also, as per study and predictions of International Energy Agency (IEA), around 27%

of global transportation energy demands are expected to be fulfilled using biomass by 2050 [14]. According to feedstocks, the biofuels are classified as first-generation (derived from edible feedstocks), second-generation (derived from lignocellulosic materials), third-generation (acquired from algal biomass feedstocks), and fourth-generation biofuels (microalgal feedstocks developed via genetic modification) [15,16]. The global biomass availability, particularly in form of lignocellulosic materials, plays an important role in reducing fossil fuel dependence by serving as a renewable feedstock for bioenergy production. Lignocellulosic biomass is the most abundant form of plant materials on earth, accounting for approximately 57% of planet's biogenic carbon [17]. This biomass is primarily sourced from agricultural residues (e.g., corn stover, wheat straw), forestry by-products (e.g., wood chips, sawdust), and dedicated energy crops (e.g., switchgrass, miscanthus). Globally, agricultural residues alone are estimated to be available at a technical potential of 1.44 billion tons annually, which could replace approximately 4.5% of global fossil fuel energy use [18,19]. Further, utilization of biomass offers several advantages such as biofuel production, energy generation, and waste valorization in the transition from fossil fuels. For instance, cellulosic ethanol is an advanced biofuel that can reduce greenhouse gas emissions by up to 85% compared to conventional gasoline, offering a more sustainable alternative for transportation [20].

In addition, numerous thermochemical and biochemical approaches are employed for generation of biofuels and biochemicals. Amongst them, pyrolysis which uses an inert environment is mostly adopted to produce bio-oil, biochar, and syngas [21,22]. However, the conventional pyrolysis requires high energy input, which impacts the overall energy efficiency of the process. Consequently, pyrolysis has evolved from conventional ways to catalytic pathways. The introduction of catalysts not only enhances reaction rates, lowers the activation energy and reduces operational energy demand [23], but also facilitates deoxygenation of bio-oil through cracking, aromatization, and hydrogenation reactions. It also produces high quality biochar and syngas, indicating improved product selectivity [24]. Therefore, exploring reaction kinetics during catalytic pyrolysis is essential, as it plays a critical role in reactor design, process optimization, understanding reaction mechanism, and scaling up to industry applications. Kinetic analysis fundamentally aims to determine the kinetic triplet (i.e., activation energy, pre-exponential factor, and reaction mechanism), which quantitatively describes the rate of the process.

Although the catalytic pyrolysis field is a broad area to explore. This review provides a focused critical analysis of the reaction kinetic principles for catalytic pyrolysis of diverse waste feedstocks such as lignocellulosic biomass, algal biomass, and plastic wastes. Primary objectives are to evaluate the widespread kinetic models, evaluate the applicability of model-free, model-fitting, and machine learning methodologies by highlighting their corresponding limitations, strengths, and applications. In addition, this review will also explore the systematic interaction between catalyst properties and kinetic parameters for various feedstocks. The review will also address the prevailing challenges and issues in catalytic pyrolysis kinetics. Lastly, this review will outline the future research directions to bridge knowledge gaps and advance the development of practical and sustainable energy solutions.

2. Fundamentals of Catalytic Pyrolysis

2.1. Process Overview

Generally, conventional pyrolysis processes which involve catalytic materials are referred to catalytic pyrolysis [25]. Catalytic pyrolysis is the prominent technique for transforming the variety of feedstocks into bio-oil and chemicals. The catalytic pyrolysis thermal behavior and energy distribution is obtained through kinetic models [26]. It requires lower operating temperatures and shows great potential for enhanced hydrogen generation from waste plastic materials [27–29]. A typical catalytic pyrolysis process set up is capable of converting solid wastes into value-added products such as bio-oil, biochar, and syngas. The process flow generally comprises feeding mechanism for biomass feedstock, reactor, electronic heating filament, and temperature control system connected to condensing unit for bio-oil generation, while non-condensable gases and biochar are collected separately [30]. Typically, fixed-bed, fluidized-bed, or circulating fluidized-bed reactors are used for conventional catalytic pyrolysis [31,32]. The catalysts are generally used via in-situ and ex-situ modes as illustrated in Figure 1. It involves biomass thermal decomposition using catalyst in the temperature ranges of 400–600 °C with normally using N_2 as working medium [33]. The study of catalytic mechanism for pyrolysis yields during terephthalate (PET) and hibiscus rosa-sinensis (HRS) co-pyrolysis revealed that inclusion of HRS increased oxygenated compounds and reduced hydrocarbons [34]. Catalytic cracking transforms the large oxygenated molecules and organic compounds into smaller ones by promoting the formation of aromatic compounds and olefins [35]. Also, interaction between varying composition of feedstocks and activity of catalysts also affects the products. For instance, Kim et al. [36] explored the catalytic pyrolysis of fungal biomass feedstocks and observed that the bio-oil derived from aspergillus contains sugar-alcohol rich chemicals, while fatty-acid rich chemicals were noted for trichoderma and penicillium bio-oils. Meanwhile, introduction of Ni-based catalyst in ex-situ form further

converted the heavy volatiles into lighter molecules, resulting into enhanced syngas generation. A significant decline in polycyclic aromatic hydrocarbon (PAH) production was observed by Tahir et al. [37] during ZnO/ZSM-5 assisted catalytic co-pyrolysis of waste cabbage and low-density polyethylene (LDPE). In-situ and ex-situ catalytic pyrolysis of lignocellulosic feedstocks was conducted to evaluate pyrolysis oil characteristics and observed that the ex-situ process demonstrated improved selectivity (98.56%), decreased oxygenated compounds (72.3%), and reduced acid contents [38].

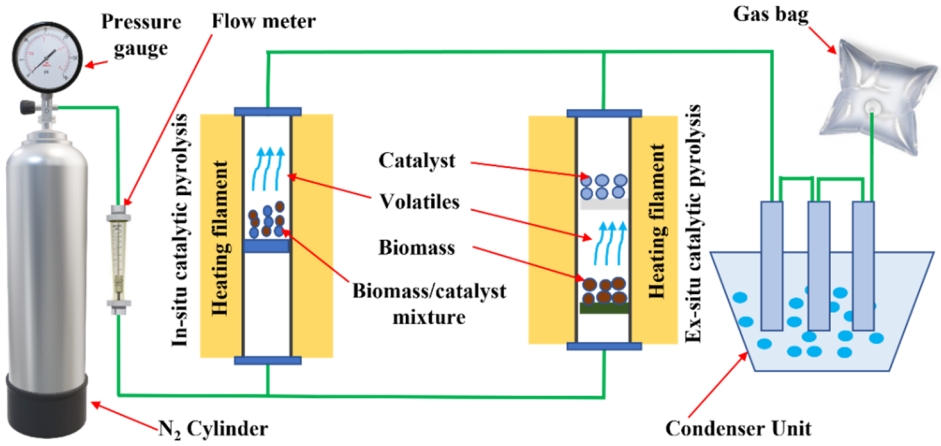

Figure 1. Process flow diagram of conventional catalytic pyrolysis processes [38].

Meanwhile, microwave-assisted catalytic pyrolysis has also emerged as an advanced substitute to conventional electronic heating for catalytic pyrolysis [39]. A schematic understanding of microwave assisted catalytic pyrolysis framework is illustrated via Figure 2. Unlike conventional catalytic pyrolysis systems, microwave heating utilizes electromagnetic radiation to internally heat biomass and catalysts using dielectric loss mechanisms [40]. It also improves the interaction between biomass and catalyst active sites resulting into higher reaction rates [41]. Additionally, microwaves encourage specific catalytic effects by activating catalysts in a different manner as opposed to external heating, resulting into improved product selectivity, bio-oil quality, and lower energy consumption [42]. Furthermore, microwave-assisted pyrolysis enables synergistic effects that can significantly influence reaction kinetics. Tiwari and Vinu [43] explored the microwave-assisted in-situ and ex-situ catalytic pyrolysis of biomass in powder and pellet forms and revealed that pellet with in-situ catalytic pyrolysis produced the highest H_2 yield, with an increased gas yield (2–10%) with palletization only. Yang et al. [44] proposed an integrated approach of reductive catalytic fractionization combined with microwave pyrolysis to improve biomass conversion as well as avoiding catalyst separation requirements and yielded 46.40 wt.% of monophenols by enhanced depolymerization of birch lignin, while syngas yields increased 1.8 times using microwave for pyrolysis. The study of synergistic effects of microwave and char-based catalysts during catalytic pyrolysis of bamboo showed that the synergy between microwave and biochar activates the catalytic active sites by promoting decarboxylation and water-gas shift reactions, resulting into diffusion of heavy components to produce higher syngas yields [45]. Similarly, enhanced H_2-rich syngas (50.22%) and lower liquid yields were observed during microwave-assisted catalytic pyrolysis of rice straw with biochar materials [46].

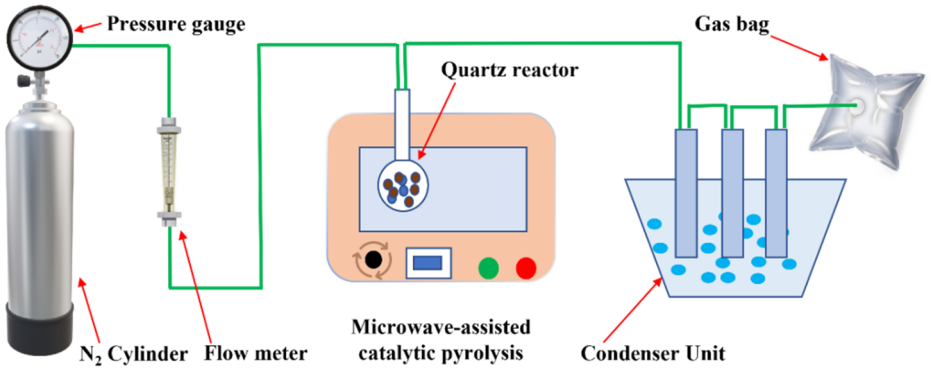

Figure 2. Schematic illustration of microwave-assisted catalytic pyrolysis process [38].

2.2. Waste Feedstocks and Their Characteristics

The selection of a suitable feedstock is primary element for the pyrolysis process. So, a fundamental understanding of feedstock characteristics is important for the catalyst selection as well as process design. The waste feedstocks generally aquatic wastes (i.e., algal biomass), agricultural and forestry wastes (i.e., lignocellulosic biomass), plastic wastes, municipal solid wastes (MSW), tires, medical waste, sewage sludge, and industrial sludge. Each waste feedstock is characterized by their unique characteristics. A summary of variety of waste feedstocks and their physicochemical characteristics is provided in Table 1. Generally, lignocellulosic biomass contains cellulose (37–50%), hemicellulose (22–32%), and lignin (15–26%), while algal feedstocks comprise of carbohydrates (3–30%), proteins (14–65%), and lipids (1–51%) [47,48]. The schematics of their respective chemical structure are illustrated in Figure 3. However, the higher oxygen present in lignocellulosic and algal biomass feedstocks tends to produce oxygenated, acidic, and low stability bio-oils, indicating for catalytic treatments for product upgradation [49].

Besides, plastic wastes containing hydrocarbons are also excellent feedstocks for chemicals and fuel recovery. Typical plastic wastes include polyethylene (PE), polypropylene (PP), polystyrene (PS), and polyethylene terephthalate (PET) [50]. The cracking of saturated hydrocarbon (H-C) polymer chains in PE and PP produces alkanes and alkenes at relatively low temperatures, while their higher volatile contents have attracted them as a suitable pyrolysis feedstock [51]. In addition, cracking of H-C chains in PS takes place through chain-end scission, producing monomers and styrene. The presence of oxygen in polymer chain of PET results into generation of significant benzoic acid and oxygenated compounds from pyrolysis [52]. MSW, which is a heterogeneous mixture of biomass, plastics, and other materials require a careful pretreatment and sorting, because presence of materials such polyvinylchloride (PVC) may result in corrosion and poisoning since it contains chlorine [53,54]. Also, composite materials of rubber, additives, and black carbon present in tires produces oil yield enriched in limonene and aromatics, high-quality char, and high calorific value gas. In addition, high ash and moisture contents in industrial and sewage sludges are the primary and major challenges towards adulteration of catalyst [55].

Table 1. Summary of physicochemical characteristics of diverse waste feedstocks.

Feedstock	MC	VM	Ash	FC [d]	C	H	N	S	O [d]	Reference
Waste tea [a]	8.20	19.80	1.00	71.0	79.30	1.70	3.40	0.20	15.20	[56]
Polystyrene [a]	0.20	98.80	0.30	0.70	90.40	8.60	0.40	-	0.60	[56]
HDPE [b]	-	98.62	1.10	0.28	75.79	11.25	0.001	0.001	11.86	[57]
LDPP [a]	-	100	-	-	85.32	14.14	-	0.54	-	[58]
Rice straw [a]	5.00	72.00	10.90	12.10	40.00	5.60	0.70	0.10	53.60	[59]
MSW [a]	0.30	57.27	34.57	7.86	43.15 [c]	4.10 [c]	1.56 [c]	0.11 [c]	51.08	[54]
Greywater algae [c]	7.50	68.20	12.60	11.70	45.30 [a]	6.50 [a]	4.80 [a]	0.40 [a]	43.00	[60]
PET [c]	-	-	-	-	62.57	4.52	0.05	0.07	32.79	[61]
Wheat straw [c]	11.24	65.75	6.67	16.34	47.94 [a]	6.01 [a]	0.23 [a]	0.05 [a]	45.77	[62]
Maplewood [c]	7.27	71.03	1.80	19.90	52.26 [b]	6.35 [b]	0.52 [b]	0.16 [b]	40.71	[63]
Chicken bone waste [a]	-	-	-	40.32	23.14	6.04	3.71	0.00	26.79	[64]
Pinewood [c]	4.11	81.24	0.25	14.40	47.41 [b]	6.19 [b]	0.17 [b]	0.65 [b]	45.58	[65]

Note: [a] dry basis; [b] dry and ash free basis, [c] as-received basis; and [d] calculated by difference.

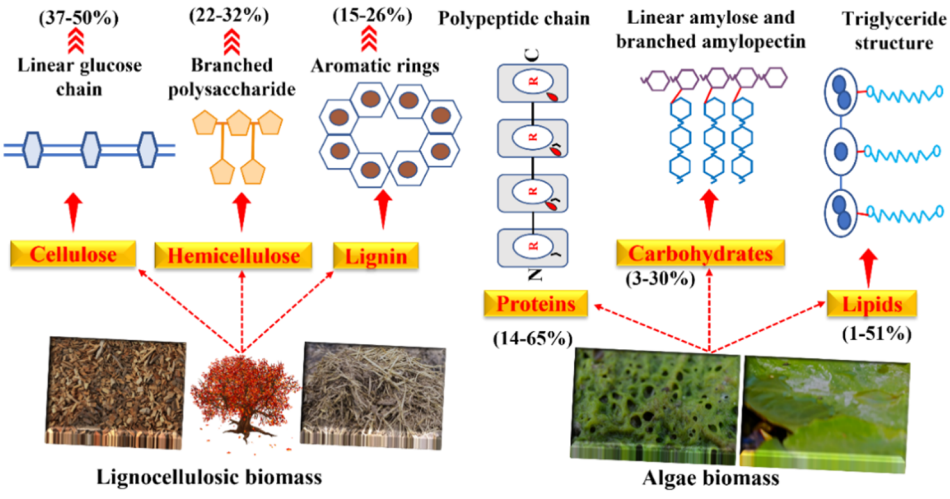

Figure 3. Schematics for chemical structures of lignocellulosic and algal feedstocks [47,48].

2.3. Catalysts and Their Functions

Catalysts play an important role in deciding the reaction pathways and distribution of final product yields. The catalysts provide active sites for specific reactions to reduce the activation energy [66,67]. Figure 4 shows the important catalyst properties which influence pyrolysis kinetics and mechanisms. Generally, catalysts are classified as acid, basic, mesoporous, and transition metal catalysts [68,69]. The acidic catalysts such as zeolites are widely employed during catalytic pyrolysis due to cracking and shape-selective reactions. Specifically, zeolites in different forms (i.e., HZSM-5, HY, Beta) have proven their effectiveness towards cracking of large hydrocarbon and oxygenated molecules, since they possess a microporous structure and have strong Brønsted acid sites [70]. Particularly, hydrogenated form of zeolites (HZSM-5) is popular for shape selectivity, aromatic hydrocarbon promotion, and enhanced production of olefins from the oxygenated compounds through oligomerization, decarboxylation, and dehydration reactions [71]. Besides, Y-zeolite based industrial catalysts such as fluid catalytic cracking (FCC) catalysts are not only effective with cracking of large molecules from waste feedstocks to gasoline type H-Cs, but are also very robust and cost effective [72].

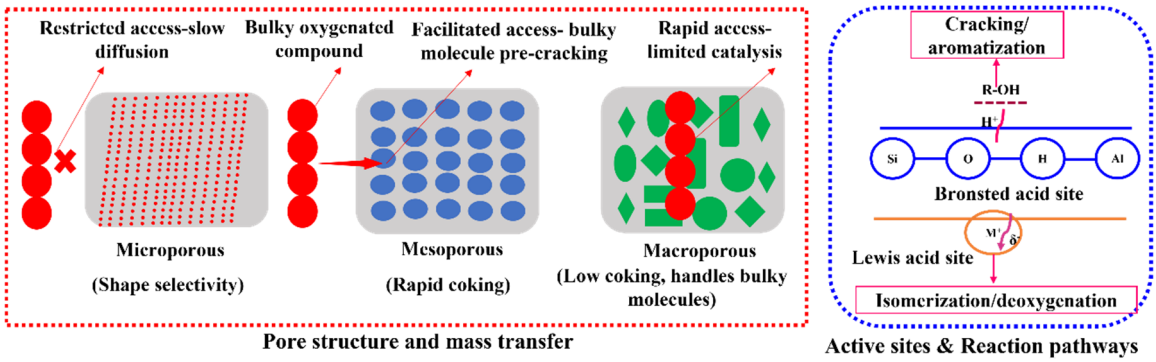

Figure 4. Key catalyst properties and their reaction pathways influencing pyrolysis kinetics and mechanisms [70,72].

In addition, basic catalysts viz. MgO, CaO, etc. are particularly used for deoxygenation, since they encourage ketonization and aldol condensation reactions to remove oxygen in form of CO_2 and H_2O [73,74]. Also, these catalysts favor carboxylation and dehydration reactions, resulting into enhanced carbon conversion efficiency as opposed to acidic catalysts. The basic catalysts work as efficient pursuer for acid components to apprehend them as stable salts. On the other hand, mesoporous catalysts have greater pore sizes in the range of 2–50 nm in comparison to zeolites. Primarily, they help to handle the bulky components derived from pyrolysis and diffuse them into small pores of zeolites [75]. Also, they help to initiate the formation of smaller intermediates from large and bulky molecules, which can be processed using microporous catalysts. Furthermore, the transition metal catalysts famous for their hydrotreating functionality are formulated from the metals (i.e., Ni, Co, etc.) supported on oxides (Al_2O_3, SiO_2) or zeolites [76,77]. These catalysts tend to eliminate oxygen in form of water via hydrodeoxygenation reactions, resulting into enhanced stability and deoxygenated bio-oil. They are also used as active members in cracking and reforming reaction [78]. Additionally, a summary of catalyst types, typical active sites, and their primary functions in catalytic pyrolysis is given in Table 2.

Further, catalytic pyrolysis involves a series of complex progressions including breakdown of macromolecules followed by catalytic alterations of the intermediates [79]. Primarily, hemicellulose, cellulose, and lignin decompose in form of volatiles and form solid residue as char. Next, secondary reactions such as cracking, decarboxylation, and aromatization takes place in presence of catalysts which provide active sites, resulting into formation of enhanced quality liquid and gas yields [80]. The acidity, pore structure, and metal sites present in catalysts governed the interaction among intermediates and influence the reaction kinetics. Remarkably, the introduction of catalyst modifies the product selectivity by encouraging PAH formation in bio-oil or reforming reactions for enhanced gas yields [81]. The reaction pathways in the catalytic pyrolysis are more clearly illustrated in Figure 5. It was reported that zeolites have better deoxidation capacity as opposed to inorganic salts and metal oxide catalysts. However, the zeolites lead to formation of coke due to low hydrogen content in biomass [82]. Also, Vuppaladadiyam et al. [83] demonstrated the reaction mechanism during catalytic pyrolysis indicating that secondary reactions such as dehydration, decarboxylation, catalytic cracking, aromatization, ketonization, reforming, and hydrogenation tend to produce aliphatic hydrocarbons, anhydro-sugars, aromatic hydrocarbons, and furans. Further, similar observations were reported by Wang et al. [84]. Further, Huang et al. [85] studied the synergistic interaction reaction mechanism among biomass pseudo components and low-density polyethylene (LDPE) and reported that the synergistic interactions in form of deoxygenation, aromatization, and Diels-Alder

reactions resulted in enhanced production of light aromatics including benzene, methylbenzene, and xylene. Also, a decline in activation energy barrier for aromatic formation (15–20 kJ/mol) was reported. Razzak et al. [86] explored the synergistic effects during catalytic co-pyrolysis of biomass and plastic wastes and observed that co-pyrolysis of algal feedstocks and plastic wastes strengthen the synergy. In-situ dual catalytic system study during biomass pyrolysis revealed that reforming reactions are intensified by CaO and Ni-char catalytic systems, leading to lower CO_2 in pyrolysis gas [87,88].

Table 2. Summary of catalyst types, typical active sites, and their primary functions in catalytic pyrolysis.

Catalyst Type	Example	Active Sites	Primary Functions in Pyrolysis	Reference
Acidic, microporous	HZSM-5, beta, HY	Bronsted acid sites	Cracking, deoxygenation (dehydration and decarboxylation), aromatization, isomerization	[89–91]
Basic/alkaline	MgO, CaO, NaOH, $Ca(OH)_2$	Basic sites	Deoxygenation (ketonization, aldol condensation), acid gas capture	[92–94]
Mesoporous	MCM-41, SBA-15, Al-MCM-41	Weak acid sites	Pre-cracking of bulky molecules, reduced coking	[95–97]
Transition metal oxides	Ni/SiO_2-Al_2O_3, Co-Mo/γ-Al_2O_3	Metallic sites	Hydrodeoxygenation, hydrogenation, reforming	[98,99]

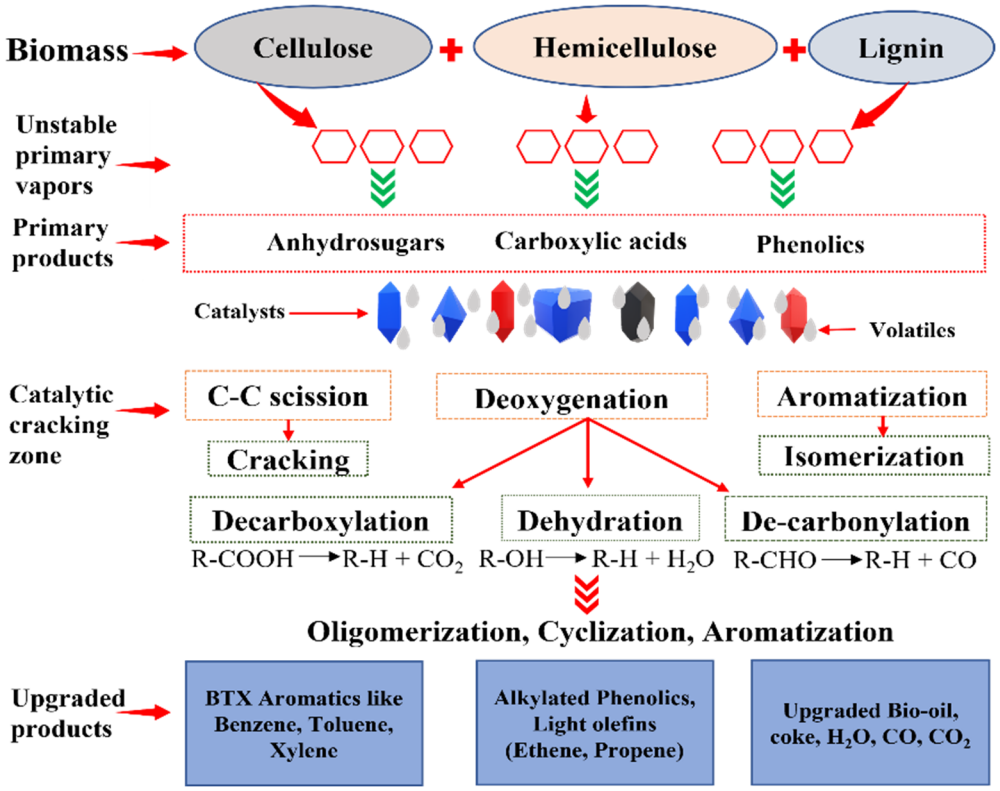

Figure 5. Reaction pathways in catalytic pyrolysis [83,84].

3. Reaction Kinetics Methodologies for Catalytic Pyrolysis

Reaction kinetics plays a key role in scaling up and commercialization of catalytic pyrolysis. The study of reaction kinetics generally involves determination of kinetic triplet (activation energy, reaction mechanism, and pre-exponential factor). The understanding of reaction kinetics is important for catalyst selection, process optimization, and reactor design [100]. The reaction kinetics for the catalytic pyrolysis is complicated and challenging to understand due to heat and mass transfer effects, complex feedstock characteristics, and a series of complex reactions occurring simultaneously [101]. This section explains the primary theoretical and experimental methodologies employed to evaluate the kinetic parameters.

3.1. Experimental Techniques

The choice of the experimental techniques adopted for the understanding of reaction kinetics requires information about decomposition rates and specific reaction pathways. Broadly, thermogravimetric analyzers (TGA) are used to monitor the solid-state kinetics. It measures the weight changes of a solid sample (i.e., a waste

feedstock mixed with catalyst) with time and temperature in a controlled environment [102]. TGA allows to analyze the devolatilization stages during thermal decomposition of a waste feedstock sample. In addition, it provides thermal decomposition data for non-isothermal and isothermal conditions [103]. Non-isothermal TGA methods are mostly used, where sample temperature is ramped gradually at constant heating rate (β). The resulting mass loss curves and their differential thermogravimetric (DTG) curves are used to analyze the decomposition stages for a particular process [104]. The model-free kinetic analysis methods consider the varying conversion rates for different heating rates and provides the activation energy (E) values without considering their reaction mechanisms. Figure 6 synthesizes a critical characteristics of catalytic pyrolysis kinetics, indicating the strong dependence of decomposition profiles on heating rate. The divergence of conversion rate ($d\alpha/dt$) curves (Figure 6b) at higher conversions underscores the multi-step nature of the reaction due to catalyst interactions. It supports the requirement of using model-free isoconversional methods over single heating rate models to accurately capture the variable E across reaction pathway, a basis for consistent kinetic explanation of complex waste feedstocks. On the other side, isothermal TGA methods ramped the sample temperature to target temperature at rapid heating rates and observe the mass loss with time [105]. Reaction rates are directly observed at particular constant temperature value using this method. However, it involves some inaccuracies due to rapid heating stage which disregards the kinetics of reaction for the time it reaches the target temperature. However, TGA can effectively provide the mass loss data required for reaction kinetics studies, it does not provide any information about the products formulated during catalytic pyrolysis. For this, TGA equipment is normally attached to other analysis systems such as gas chromatography (GC), mass spectroscopy (MS), GC-MS, and Fourier transform infrared (FTIR) spectroscopy [106].

While TGA provides fundamental and reproducible decomposition data, it is crucial to critically interpret the derived kinetic parameters within the context of their idealized experimental conditions. The small sample mass, fine particle size, and uniform heating in TGA minimize intra-particle and inter-phase heat and mass transfer resistances, allowing the measurement of kinetics that approach the intrinsic chemical reaction rates. However, real catalytic pyrolysis reactors (e.g., fluidized beds, screw conveyors) operate under significant transport limitations, where bulk heating, volatile diffusion, and catalyst-contact efficiency govern the observed global rates. The kinetics extracted from TGA are therefore more accurately termed apparent kinetics for that specific analytical configuration. Directly applying these parameters to predict behavior in large-scale reactors can be misleading, as the apparent activation energies and reaction models do not account for the dominant transport phenomena and complex hydrodynamics at scale. Consequently, TGA serves as an essential tool for initial screening and mechanistic insight under controlled conditions, but its data must be consciously integrated with pilot-scale validation or coupled with reactor models that explicitly resolve transport effects to bridge the lab-to-industry gap.

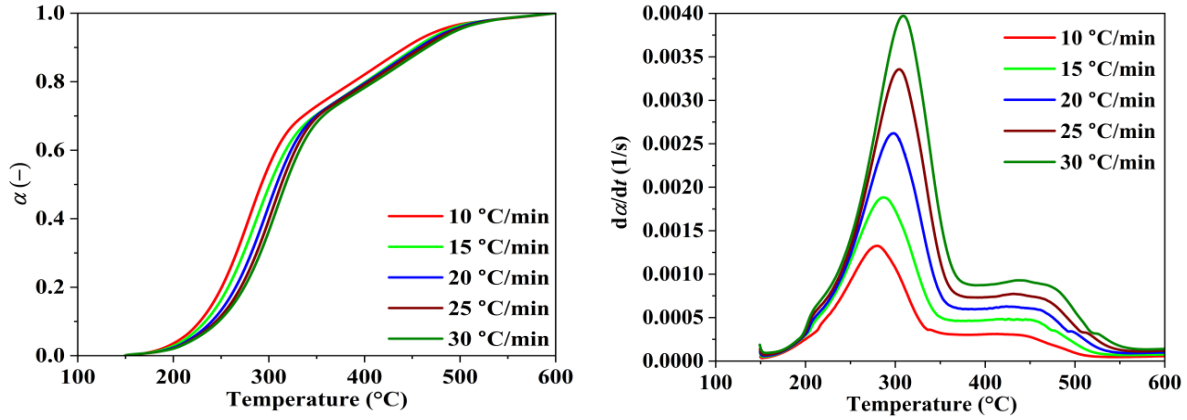

(**a**) Conversion curves (**b**) Conversion rate curves

Figure 6. Conversion and conversion rate curves for non-isothermal TGA methods [16].

3.2. Data Processing and Model Fitting

The experimental data derived from non-isothermal and isothermal TGA methods is further processed to extract the kinetic parameters viz. activation energy (E), reaction mechanism ($f(\alpha)$), and pre-exponential factor (A). Kinetic analysis uses α and conversion rates for further processing of the TGA experimental data. α can be calculated using following expression [107]:

$$\alpha = \frac{m_0 - m_t}{m_0 - m_f} \quad (1)$$

Here, m_0, m_t, and m_f represent the original, instantaneous, and final values of sample mass in the defined temperature stages. For an individual thermal decomposition process, α varies in the range of 0 to 1. Although, the kinetic parameters are not evaluated normally at start and end of the process, since no conversion rates can be determined at these instants [108]. Further, the conversion rates rely on temperature (T) dependent Arrhenius reaction rate constant (k) and α dependent reaction mechanism [109], which is generally expressed in form of Equation (2).

$$\frac{\mathrm{d}\alpha}{\mathrm{d}t} = k(T)f(\alpha) = Ae^{\left(\frac{-E}{RT}\right)}f(\alpha) \quad (2)$$

where: R denotes universal gas constant (J/mol·K), $f(\alpha)$ signifies reaction mechanism, A represents pre-exponential or frequency factor, E signifies activation energy, and t represents time.

3.2.1. Determination of Activation Energy

Various approaches of kinetic analysis are used to determine activation energy by using Equation (2) in their modified differential and integrated forms. These are generally classified as model-free and model-fitting methods. Model-free kinetic analysis approaches are commonly employed for examining thermal degradation behavior during pyrolysis without taking into consideration of their reaction models [110]. For this, reaction rates are evaluated with respect to constant α for different β values to determine activation energy (E). Also, it considers the reaction rate as a function of temperature (T) at constant α value. Model-free methods provide E profiles which are further used to decide the reaction mechanisms and pre-exponential factor (A) across α, presenting valuable efforts towards optimization of process and reactor design. Generally, model-free methods are classified as differential (i.e., Friedman) and integral methods viz. Kissinger-Akahira-Sunose (KAS), Starink, Boswell, and Ozawa-Flynn-Wall (FWO) [65]. The differential isoconversional Friedman method has proven its accuracy in E calculations, while integral methods are used with certain integral approximations as they lack exact solution unlike Friedman method [111]. Also, model free methods involve potential errors due to experimental limitations (i.e., experimental data) and data interpretation challenges for vastly heterogeneous schemes. Despite these limitations, isoconversional model free methods provide an important reaction kinetics pathway for the catalytic pyrolysis of biomass. The common mathematical expressions for these differential and integral methods are provided in Table 3 [108,112].

Table 3. Commonly used differential and integral model-free kinetic analysis methods.

Type	Method	Empirical Correlation	Source
Differential	Friedman	$\ln\left(\frac{\mathrm{d}\alpha}{\mathrm{d}t}\right) = \ln[f(\alpha)A] - \frac{E}{RT}$	[113]
Integral	KAS	$\ln\left(\frac{\beta}{T^2}\right) = \ln\left[\frac{AR}{Eg(\alpha)}\right] - \frac{E}{RT}$	[114]
	FWO	$\ln(\beta) = \ln\left[\frac{AE}{Rg(\alpha)}\right] - 5.330 - 1.0518\left(\frac{E}{RT}\right)$	[115]
	Starink	$\ln\left(\frac{\beta}{T^{1.92}}\right) = \text{constant} - 1.0008\left(\frac{E}{RT}\right)$	[63]
	Boswell	$\ln\left(\frac{\beta}{T}\right) = \text{constant} - \left(\frac{E}{RT}\right)$	[108]

These differential and integral methods are used to draw the isoconversional plots at multiple heating rates. The slopes of these linear isoconversional plots are used to calculate activate energy variations, while the intercept values are used for pre-exponential factor determination with varying α [116]. Furthermore, the main advantage of using the model-free methods is that they provide separate E with α values. A nominal change in E with α signifies that the reaction is single step. But, a very significant variation in E values with α indicates towards multi-step and complex reaction. Such incidents are generally noticed in cases where catalysts are used during pyrolysis of waste feedstocks.

Complementary to model free methods, kinetic analysis of catalytic pyrolysis can also be performed using model-fitting approach. Model-free techniques, such as Friedman, FWO and KAS, estimate activation energy without specifying reaction mechanisms, focusing on empirical determination from thermal analysis data. Meanwhile, model-fitting methods involve assuming reaction models (e.g., 1st-order, nth-order, nucleation, etc.) and adjusting parameters to best fit experimental data. These models provide mechanistic insights but may oversimplify the inherently complex reactions of biomass. However, model-fitting can simulate the explicit

pyrolysis stages or catalyst effects in a better way to predict kinetic parameters. Coats-Redfern (C-R) method is the most common and widely used model-fitting approach. Largely, it is considered as an integral approach of kinetic analysis as it uses integral form of theoretical reaction models to evaluate *E*. Also, a major difference between model-free integral methods and C-R method is that it considers only single heating rate and provides one value of *E* and *A* for whole process, while model-free methods can provide multiple *E* and *A* values at particular α and also uses multiple heating rates (i.e., usually ≥3). The generalized C-R method's empirical correlation is represented by Equation (3) [117].

$$\ln\left[\frac{g(\alpha)}{T^2}\right] = \ln\left[\frac{AR}{\beta E}\left(1-\frac{2RT}{E}\right)\right] - \frac{E}{RT} \tag{3}$$

Here, $g(\alpha)$ denotes the integral reaction mechanism, which is evaluated using the master plot analysis discussed in subsequent subsection.

3.2.2. Determination of Reaction Mechanism and Pre-Exponential Factor

Once the values of *E* are determined using model-free methods, the average activation energy (E_0) values are generally used for deciding the suitable reaction model. For this, master plot analysis is generally employed which usually follows a single-step approach. Master plots use the integral and differential form of theoretical reaction model curves to compare with experimental curves [118]. For instance, y(α) master plots use the differential form of theoretical reaction models, while Z(α) master plots use a combined approach where they consider both integral and differential theoretical reaction models for comparison and it also do not require prior knowledge of *E* [108,119]. Basically, the conversion rate expression in Equation (2) formulates the basis of y(α) master plot analysis and used in following form [120]:

$$\mathrm{y}(\alpha) = \left(\frac{\mathrm{d}\alpha}{\mathrm{d}t}\right) e^{\left(\frac{E}{RT}\right)} = Af(\alpha) \tag{4}$$

Here, thermogravimetric experiments help to provide temperature (*T*) and conversion rate (dα/d*t*) values, while *E* values are obtained using the slopes of isoconversional plots drawn from expressions listed in Table 3. It assumes that *E* values do not vary much across α and uses average value of activation energy (E_0). Also, it considers the average values for pre-exponential factor (A_0) instead of separate *A* for individual α [121]. Additionally, the reaction models vary in magnitude based on their type and nature (i.e., nucleation, order-based, sigmoidal, power law) [122]. Therefore, theoretical reaction models are normalized at a reference value (say at α = 0.5), which redevelops Equation (4) in following form [123]:

$$\mathrm{D}(\alpha) = \frac{\mathrm{y}(\alpha)}{\mathrm{y}(0.5)} = \frac{\left(\frac{\mathrm{d}\alpha}{\mathrm{d}t}\right) e^{\left(\frac{E_0}{RT}\right)}}{\left(\frac{\mathrm{d}\alpha}{\mathrm{d}t}\right)_{0.5} e^{\left(\frac{E_0}{RT_{0.5}}\right)}} = \frac{f(\alpha)}{f(0.5)} \tag{5}$$

In Equation (5), D(α) denotes the normalized y(α) master plot, and the $f(\alpha)/f(0.5)$ signifies formulations of theoretical reaction model curves, which are compared with experimental curves to determine reaction mechanisms. A list of common theoretical solid-state reaction models is presented in Table 4.

Table 4. Commonly used solid-state reaction mechanism in their differential and integral forms [110,124].

Reaction Model	Notation	Differential Form $f(\alpha)$	Integral Form $g(\alpha)$
Exponential growth models			
Power law	P2/3	$[2/3]\ \alpha^{-1/2}$	$\alpha^{3/2}$
Power law	P*n*	$n\ \alpha^{(n-1)/n}$	$\alpha^{1/n}$
Diffusion processes			
1-D diffusion	D1	$[1/2]\ \alpha^{-1}$	α^2
2-D diffusion	D2	$[-\ln(1-\alpha)]^{-1}$	$[(1-\alpha)\ln(1-\alpha)]+\alpha$
3-D diffusion	D3	$[3/2]\ (1-\alpha)^{2/3}[1-(1-\alpha)^{1/3}]^{-1}$	$[1-(1-\alpha)^{1/3}]^2$
Nucleation reactions			
Avrami-Erofeev	A*n*	$n(1-\alpha)\ [-\ln(1-\alpha)]^{(n-1/n)}$	$[-\ln(1-\alpha)]^{1/n}$
Order-based reactions			
First-order	F1	$(1-\alpha)$	$-\ln(1-\alpha)$
*n*th-order	F*n*	$(1-\alpha)^n$	$[(1-\alpha)^{1-n}-1]/(n-1)$
Shrinkage models			
Contracting cylinder	R2	$2(1-\alpha)^{1/2}$	$1-(1-\alpha)^{1/2}$
Contracting sphere	R3	$3(1-\alpha)^{3/2}$	$1-(1-\alpha)^{1/3}$

Note: *n* notifies the order of the reaction.

In addition to that, Z(α) master plots are obtained by using the integral form of conversion rate expression and can be expressed in form of Equation (6) after various integral approximations. Then, Z(α) function is obtained by using subsequent rearrangements in form of Equation (7) [125].

$$g(\alpha) = \frac{AE}{R\beta} e^{(-x)} \left[\frac{\pi(x)}{x}\right] \tag{6}$$

$$\mathrm{Z}(\alpha) = f(\alpha)g(\alpha) = \left(\frac{\mathrm{d}\alpha}{\mathrm{d}t}\right) T_\alpha^2 \left[\frac{\pi(x)}{T_\alpha \beta}\right] \tag{7}$$

Here, $x = E/RT$ and function $\pi(x)$ denotes the Arrhenius integral approximation function, which is defined using following expression [126]:

$$\pi(x) \approx \frac{x^3 + 18x^2 + 88x + 96}{y^4 + 20y^3 + 120y^2 + 240y + 120} \tag{8}$$

where, the term $[\pi(x)/T_\alpha\beta]$ in Equation (7) usually ignored while drawing master plot curves, since it does not affect Z(α) function considerably. Also, it is used in normalized form as I(α) for similar reasons and expressed as followings after rearrangements:

$$\mathrm{I}(\alpha) = \frac{\mathrm{Z}(\alpha)}{\mathrm{Z}(0.5)} = \frac{f(\alpha)g(\alpha)}{f(0.5)g(0.5)} = \frac{\left(\frac{\mathrm{d}\alpha}{\mathrm{d}t}\right) T_\alpha^2}{\left(\frac{\mathrm{d}\alpha}{\mathrm{d}t}\right) T_{0.5}^2} \tag{9}$$

Here, term $f(\alpha)g(\alpha)/f(0.5)g(0.5)$ denotes the theoretical form of reaction mechanism, while right hand side term is drawn from experimental data. Then, a comparison of shape similarity and closeness between theoretical and experimental reaction models is established to select the suitable reaction model. Moreover, sometimes it is difficult to observe and decide the proper order (n) of the reaction model used. For this, mathematical regression analysis is used in form of χ^2-minimization or RSS-minimization [22]. After determining the reaction model with correct order (n), the intercept values from the isoconversional plots are used to determine A values with α.

While, master plot analysis provides a systematic framework for mechanism selection, its application to complex systems such as catalytic pyrolysis comprises inherent subjectivity. The assignment of a reaction mechanism can be non-unique, as multiple theoretical models (differential or integral) may show similar curve shapes, resulting into reasonable but unclear fits. This ambiguity is often intensified by sensitivity of data preprocessing such as smoothing of DTG curves to reduce noise, and the range of T and α. Consequently, mechanism selection should not solely rely on visual inspection for matching curves. It requires a complimentary statistical regression such as χ^2-minimization or RSS-minimization to validate against independent experimental evidence or physicochemical reasoning regarding the likely catalytic cracking or decomposition pathways. Figure 7 integrates the methodological discussion into a novel, decision focused framework.

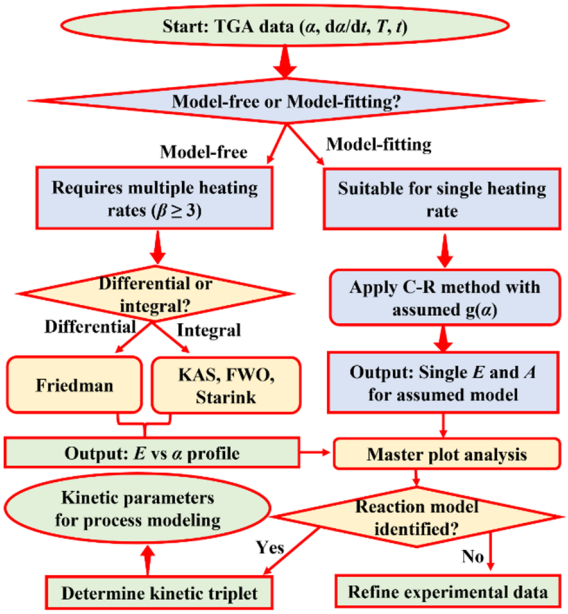

Figure 7. Decision flowchart for selecting kinetic analysis methodologies in catalytic pyrolysis [127].

Therefore, in order to carry out a rigorous kinetic study of catalytic pyrolysis, one should begin with choosing a particular experimental technique (such as TGA to analyze decomposition rate data) followed by processing the experimental data using isoconversional methods to obtain *E* profiles. It helps to decide reaction complexity. These observations are further followed by master plot analysis to determine the suitable reaction mechanism and its correct order following regression analysis methods. Lastly, it involves calculation of *A* using intercept values at each α.

Various studies in the literature have used different approaches for conducting kinetic analyses under variable experimental conditions. For instance, kinetic analysis during pyrolysis of chlorella vulgaris was explored using model-free methods, including FWO, KAS, Starink, and Tang and observed the activation energies in the range of 138.7–141.5 kJ/mol for a conversion range of 0.1–0.9 in the temperature range of 150–600 °C for three heating rates were used as 10, 20, and 30 °C/min [128]. Further, co-pyrolysis of industrial hemp waste (IHS) and polyvinyl chloride (PVC) under 10, 15, and 30 °C/min conditions yielded average activation energy of 154.37 kJ/mol using Friedman method. However, the pseudo-components P-H, P-C, P-L, P-P for IHS+PVC exhibited mean activation energy of 172.28, 186.76, 110.7, 286.06 kJ/mol, respectively [129]. A thermokinetic study using KAS and FWO methods during pyrolysis of hydrothermally pretreated pumpkin (PC) and hemp (HC) oil cakes revealed that the *E* values varied in the range of 93.6–529.9 kJ/mol for PC and 71.3–669.9 kJ/mol for HC [130]. Meanwhile, kinetic analysis of PMMA/H-β zeolite using Gaussian deconvolution yielded E_0 values as 84.9, 128.2, 113.1 kJ/mol for P/B-91, P/B-82, and P/B-73, respectively [131]. These observations reported in the literature visually synthesize how varying experimental conditions can lead to dissimilar results.

3.2.3. Machine Learning for Kinetics

In addition to conventional methods, machine learning (ML) has emerged as a powerful computational approach for conducting kinetic analysis and predicting product yields from complex pyrolysis data [132]. ML plays a key role in handling large, complex TGA experimental datasets and identifying the non-linear correlations which are usually overlooked in conventional kinetic analysis methods [133]. A standard ML workflow comprises data collection, followed by algorithm training using linear regression models, Gaussian process, and artificial neural network (ANN) regression models [134]. Then, these models are validated to predict the kinetic parameters, as illustrated in Figure 8. This emphasizes that ML is not a one-time fitting exercise but an iterative process where model failures inform targeted new data generation. Also, ML enables the development of dynamic and adaptive models which integrate the process variables, catalyst properties, and feedstock heterogeneity, resulting into enhanced accuracy of control, prediction, and optimization [135].

Practical case studies demonstrate the successful application of diverse ML algorithms across various feedstocks. For instance, study of catalytic pyrolysis kinetics explored using Gaussian process regression (GPR) revealed that the GPR model predicted the thermo-kinetic parameters with high accuracy ($R^2 > 0.999$) [136], ensemble methods like extreme gradient boosting (XGBoost) to optimize liquid oil yield predictions from plastic waste ($R^2 = 0.85$) [137]. Beyond catalysis, ML has shown versatility in related domains, such as hydrogen release kinetics in alloys using evolutionary deep neural network (EVoDN2) [138] and modelling biomass pyrolysis via multi-variative adaptive regression splines (MARS) to closely match activation energies ($R^2 = 0.9974$) [139]. Further applications include comparing ANN performance ($R^2 = 0.994$) against traditional model-free and model-fitting methods [140] and utilizing random forest models to predict activation energies for diverse feedstocks with high accuracy ($R^2 = 0.9964$) [141]. Collectively, these practical cases underscore ML's empirical strength in pattern recognition and yield prediction [133,142].

However, a critical perspective must accompany these demonstrations of predictive power. A primary focus on high R^2 values can overshadow significant limitations, including model transparency, overfitting risks, and a lack of mechanistic insight. ML models particularly complex architectures like deep ANNs, often function as black boxes, where the derived parameters (viz. apparent activation energy, reaction order, frequency factor) may serve as flexible empirical fitting coefficients rather than possessing direct physical or mechanistic meaning [132,134]. This opaqueness challenges the extraction of fundamental chemical insight. Additionally, these models are susceptible of overfitting, especially with limited or noisy training data, which can compromise their generalizability beyond original dataset [133,143].

Therefore, while ML is an effective tool for empirical correlation and prediction, its role should be distinguished from methods that yield physically interpretable kinetic triplet. Future advancements should prioritize strategies that enhance interpretability and physical grounding. It includes development of hybrid models that embed fundamental constraints such as mass balance, Arrhenius-type relationships, within the ML architecture and employing interpretability techniques to elucidate which input features most considerably influence predictions [132,144]. Through such approaches, ML can evolve from a purely empirical fitting tool to a

complementary component of a multi-scale modelling framework, bridging data-driven patterns with mechanistic understanding for more reliable scale-up and optimization.

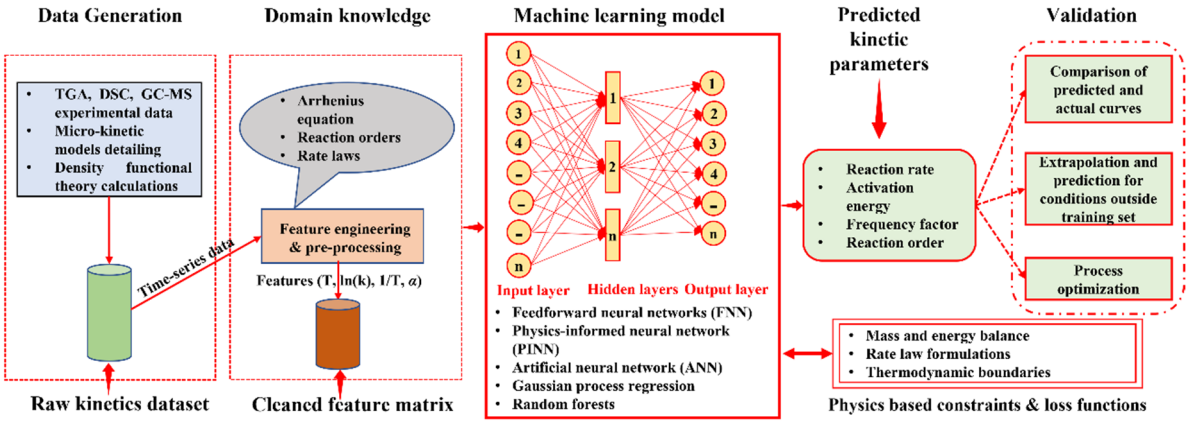

Figure 8. Machine learning workflow for kinetic modelling [145].

3.3. Comparative Reliability and Applicability

Pyrolysis characteristics and kinetics were explored by several researchers using model-fitting, model-free, and machine learning approaches. The comparative analysis of model-free methods showed that KAS and Vyazovkin methods follow similar trends of E variations due to temperature integral approximations, while Friedman showed different E variation trends since it does not contain systematic error caused by various integral approximations. Meanwhile, model-fitting C-R method exhibited insignificant variations since it considers reaction as single-step [146] Bharti et al. [147] also used similar approaches during pyrolysis of microalgal feedstock and observed E_0 values as 146.78, 148.86, and 147.11 kJ/mol with KAS, FWO, and Vyazovkin models, while it was noted that E values varied significantly based on the reaction mechanism, when C-R method was used. In another study, model-free (KAS, FWO, Friedman, Starink, and Vyazovkin) and DAEM model-fitting methods were used to explore the finger millet pyrolysis kinetics and observed E_0 values ranging from 167–175 kJ/mol, while one-way ANOVA revealed that there are no statistical differences ($p = 0.9353$) in E_0 values calculated from different methods. Meanwhile, development of ANN based ML model accurately predicted the mass loss (%) with an R^2 of 0.9995 [140]. Sbirrazzuoli [148] performed the kinetic analysis of complex chemical reactions by coupling model-free and model-fitting analyses. The advanced non-linear isoconversional (NLN) method revealed increasing E-dependency (35–103.6 kJ/mol) and ln$A$-dependency (4.72–30.78 s^{-1}) from competing reactions, while consecutive reaction shows decreasing dependency, while independent reactions exhibited a more complex (increasing/decreasing) dependency with α. A critical analysis of possibility of using model-free methods for kinetic analysis and developed conversion functions to determine compensation effect parameters, stating obvious differences in kinetic parameters due to inherent experimental errors, errors in evaluation of activation parameters, and deviation from linearity of ln$A$ vs. E regression [149].

4. Kinetic Models for Catalytic Pyrolysis of Specific Waste Feedstocks

Optimization of catalytic pyrolysis for different waste feedstocks faces challenges during suitable kinetic model development. Since, it involves a network of complex reactions, occurring at interface of feedstock components and catalysts at elevated temperatures [150]. This complexity arises from the multicomponent nature of waste materials as well as dynamic interaction amongst volatiles and active sites of the catalysts [151]. Therefore, current state of kinetic modelling is represented in this section to highlight feedstock specific challenges, modelling approaches, and catalytic effects.

4.1. Lignocellulosic and Algal Biomass

The lignocellulosic feedstock structure involves three primary components such as hemicellulose, cellulose, and lignin. These components react differently during thermal decomposition, which poses a considerable challenge during kinetic analysis. The single step kinetic models often fail to consider the overlapping thermal degradation regimes of these components. It is a noticeable fact that the hemicellulose degradation takes place at lower temperatures (220–325 °C), cellulose at relatively higher (315–400 °C), and lignin decomposes throughout the reaction at low degradation rates with temperatures starting from 160 °C to end of process [152,153]. This

create overlapping reaction profiles which are not easy to deconvolute. Now, these limitations are advanced through deconvolution modelling approach, which breaks the decomposition curves into its pseudo-components. A good performance in deconvolution was reported using Fraser-Suzuki deconvolution technique, which provides a good fitting accuracy to TGA data. In addition, algae feedstocks are comprised of proteins, carbohydrates, and lipids which decompose in the temperature ranges of 205–310 °C, 160–470 °C, and 200–635 °C [154,155]. This multi-stage and overlapping regime decomposition behavior of algae feedstocks requires selecting multiple temperature regimes for kinetic modelling, where each temperature regime provides separate kinetic parameters. It has been reported in the literature that algae feedstocks demonstrate lower *E* values as compared to lignocellulosic feedstocks [156].

Meanwhile, a significant effect of catalysts is evident over kinetic triplets during pyrolysis, showing separate reaction pathways and lower *E* values. For instance, *E* values and reaction models are significantly affected by the inclusion of acid catalysts such as HZSM-5 during pyrolysis of biomass feedstocks [95,157]. A significant decline in *E* barrier by 30.54% for xylan, 6.73% for cellulose, and 14.75% for lignin was observed during catalytic pyrolysis of model biomass compounds [100]. It indicates towards the requirement for the component specific kinetic modelling during catalytic pyrolysis. Further, different reaction models are followed for the individual biomass component. It was reported that the pseudo-components (hemicellulose and lignin) obey F3 reaction model, while cellulose follows the random scission mode [158], while these reaction models are altered for catalytic pyrolysis and showed diffusion mechanisms as most favorable models. Further, catalysts containing alkali metals such as potassium compounds further encourage the cross-linking reactions owing to decline in char yield as well as *E* values for the cellulose rich biomass feedstocks, while making the pyrolysis reaction more complex [159].

Further, lumped kinetic modelling approach considers the practical framework to predict distribution of products by tracking the individual chemical reaction. These lumped models form discrete lumps to describe the concerned reaction networks [160,161]. These lumped approaches are particularly converted into complex formulations for catalytic pyrolysis, since it involves secondary cracking reactions which encourage formation of H-C, water, and light gases [162]. Therefore, a careful consideration of catalyst to biomass ratios is needed to control the secondary reactions. Models need to consider enhanced aromatization and deoxygenation reactions at higher catalytic loadings. In addition, these lumped models should consider the N-containing compounds for proteins [163]. It has been observed from lumped model kinetic analysis that the *E* values vary in the order of gas > bio-oil > char, indicating raising energy requirements in these pathways.

4.2. Plastic Waste

The pyrolysis of plastic waste is governed by random scission and end-chain scission models during kinetic models. The polymer chain breakage resulting into reduced molecular weights and varying size fragments is assumed via random scission models [164]. The polymers (i.e., PP, PE) promoting random cleavage of C-C bonds are analyzed through random scission models. In addition, end-chain scission models involving sequential elimination of monomers from chain ends results into intermediate fragments of monomers. PS degradation which yields higher styrene monomers is governed by the end-chain scission models [165]. However, random scission results into a broad distribution of product yields with lighter liquids and high gases, while monomer recovery is ideal in end-chain scission models. Meanwhile, the real-world plastic wastes exhibit the higher reaction complexity of kinetic modelling since it contains mixed polymers which affect the scission behavior during pyrolysis [166].

Additionally, plastic pyrolysis reaction kinetics is significantly altered using acid catalysts such as zeolites and FCC catalysts in form of enhanced carbonium ion intermediates. Also, a significant reduction in *E* values was noticed from catalytic pathways as opposed to non-catalytic pyrolysis [167]. Formation of carbocation intermediates must be considered during kinetic modeling of these plastic wastes to analyze the β-scission and hydrogen transfer reactions. Further, kinetic triplet is affected by concentration and strength of acid sites in catalysts, because stronger active sites encourage the widespread cracking at relatively low temperatures. For instance, catalytic cracking mechanism for polyolefins begins through polymer chain protonation at Brønsted acid sites, then these reactions further break the polymer chain into smaller H-C via β-scission reactions [168,169]. Coke formation which blocks the active sites considers the catalyst deactivation during kinetic modelling. It has been reported from several studies that the inclusion of catalysts during plastic pyrolysis requires 30–50% lesser *E* compared to non-catalytic pyrolysis, indicating higher decomposition rates for catalytic systems [100,170].

Further, due to varying chain structure, stereochemistry, and bond cleavage energies for different polymer types showed significant difference in kinetic behavior during catalytic pyrolysis of plastic wastes. For instance, PP and PE demonstrate similar catalytic degradation behaviors. However, lower *E* required for PP, since it possess ternary carbons. Meanwhile, HZSM-5 assisted catalytic pyrolysis of PP obeys F1 model with lower *E* values

varying in the range of 150–180 kJ/mol as compared to non-catalytic pyrolysis (200–250 kJ/mol) [171]. Similarly, catalytic pyrolysis for PS kinetic modeling replicates end-chain scission reactions to produce monomers. Also, thermal decomposition kinetics of PS is affected by aromatic rings in form of resonance stabilization [172]. Besides, PET offers extra reaction complexity as it has higher oxygen content. This leads to consideration of dehydration and deoxygenation reactions during kinetic modelling. The lower *E* requirements in PET pyrolysis are particularly referred to availability of esters linkages [173].

4.3. Mixed Feedstocks

Mixed feedstocks such as plastic-biomass mixtures during pyrolysis demonstrate non-additive behavior with a significant deviation between reaction rates and distribution of product yields compared to individual components [174]. The synergistic effect is quantitatively defined as a significant deviation from the weighted additive behavior of individual feedstocks. Generally, this deviation is most rigorously identified through key kinetic parameters, such as measurable reduction in activation energy, or a change in reaction mechanism compared to the linear combination of individual component kinetics. While, synergy indicates the important interactions, it is important to distinguish true chemical interactions from artifacts of experimental certainty. Apparent synergy can arise from measurement errors in TGA, heat/mass transfer limitations that differentially affect blends, or statistical variability in product analysis. Therefore, claims of synergy should be supported by rigorous statistical analysis, reproducibility across experimental setups, and mechanistic evidence, ensuring the observed deviation exceeds the cumulative experimental error of the measurements. The synergistic effects between mixed feedstocks show significant variations in kinetic parameters. Commonly, synergistic effects are observed in terms of *E* reductions, due to stabilization of intermediates from biomass pyrolysis and plastic radicals [175]. For example, a significant reduction in *E* values to 24.31 kJ/mol owing to synergistic effects during co-pyrolysis of coal and microalgae feedstocks was observed as compared to coal (31.11 kJ/mol) pyrolysis [176]. Alterations in reaction mechanisms also indicate enhanced synergy of mixed-feedstock pyrolysis. Like, reaction mechanism changed from diffusion mechanism to reaction-controlled mechanism for biomass and plastic feedstock mixtures. However, blending ratio plays important role to decide the extent of synergy between mixed feedstocks [177]. Therefore, an extra consideration of terms such as interaction coefficients and coupled reaction becomes necessary during kinetic modelling.

Bamboo and oakwood co-pyrolysis with PP and PS revealed that the activation energy significantly decreased from when a mixing ratio of 4:1 was used. Particularly, highest decrease was observed for bamboo and PS mixture from 217.59 kJ/mol to 149.81 kJ/mol, indicating positive synergistic effect [178]. Study of synergistic effects during catalytic co-pyrolysis of sludge and chlorella with mixing ratio of 1:3 using CaO/K_2FeO_4 demonstrated lower carboxylic acids and nitrogen chemicals with a decline by 17.84% and 54.62%, respectively [179]. Li et al. [180] explored the thermal behavior and K-Fe synergistic effects during catalytic pyrolysis of Chinese herb residues and observed a K-Fe derived catalytic synergistic effect in terms of reduced activation energy from 186.1 kJ/mol to 149.6 kJ/mol, while increased H_2 yield was also observed from 51.46 L/kg to 135.36 L/kg. In addition, tobacco straw and LDPE co-pyrolysis in presence of HZSM-5/graphite felt composite catalyst yielded 41.47% of MAHs at a mass ratio of 80%, indicating combined synergistic effects from pore acidity of catalyst and microwaves [181]. These discrepancies in literature demonstrates that divergent experimental conditions often yield conflicting results.

Additionally, several formidable challenges related to contribution of pseudo-components and their interaction in deconvolution are presented by mixed feedstocks during kinetic analysis [182]. Primarily, overlapping regions of thermal decomposition owing to simultaneous degradation of multiple components presents the primary challenge. This complexity is largely noticed in the MSW which are generally comprised of various plastics, biomass, textiles, and inert materials [183]. Multi-step kinetic reaction models consider such conditions separately to analyze the decomposition and interaction behavior [184]. For example, five different reaction stages were defined to evaluate the separate kinetic triplet in each reaction stage during co-pyrolysis of microalgae and sewage sludge [185]. During elimination of moisture and light volatiles, F1 model with *E* values varying in the range of 15.07–42.34 kJ/mol was seen, while major devolatilization regime showed comparatively greater range of *E* variations as 62.69–78.86 kJ/mol. Besides, use of isoconversional approaches can efficiently tackle these complex situations by providing the insights into limiting steps and shifting conversion rates with progress of reaction [186,187]. It was observed from isoconversional techniques that *E* values varied considerably with α during pyrolysis of mixed feedstocks, while individual pure feedstocks showed very insignificant variations in *E* values. A comprehensive comparison of kinetic parameters during kinetic analysis of catalytic pyrolysis for diverse feedstocks in presented in Table 5. Additionally, Figure 9 provides a cross-feedstock meta-analysis, revealing a key literature insight, the range of *E* for plastics is significantly lower than for heterogeneous biomass feedstocks.

It underscores that the feedstock identity dictates kinetic simplicity. Crucially, it highlights outlaying position of mixed feedstocks, which often show lower *E* than pure feedstocks, suggesting kinetic synergy. Further, Table 6 presents a summary of synergistic effects observed for the co-pyrolysis of mixed feedstocks. Catalytic pyrolysis kinetics for diverse feedstocks still remains a challenging task due to developments in waste valorization methods. Also, multicomponent nature of feedstocks is treated using deconvolution methods. Still, a big area of exploration lies in capturing synergistic interactions of mixed feedstocks and evolution of catalytic activity during pyrolysis.

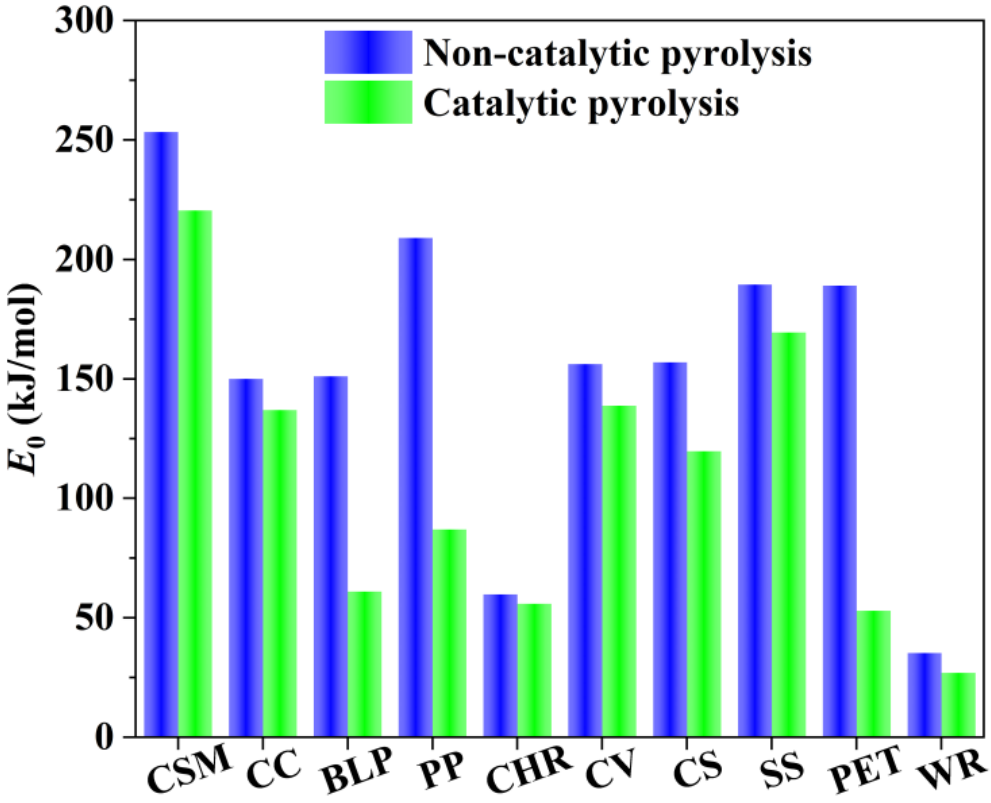

Figure 9. Comparative analyses of activation energies for catalytic pyrolysis of different feedstocks viz. cotton swab and non-woven mask (CSM) [188], corncob (CC) [189], Bamboo and LDPE (BLP) [190], PP [191], Chinese herb residue (CHR) [192], chlorella vulgaris (CV) [193], caster seeds (CS) [194], sewage sludge (SS) [195], PET [196], and waxy residue (WR) [197].

Table 5. Comprehensive comparison of kinetic parameters for catalytic pyrolysis of diverse feedstocks.

Feedstock	Catalyst	Catalyst Type	Kinetics Method	E_0 (kJ/mol)	Reaction Mechanism	Reference
Pineapple peel	Ni-Fe	Supported metal	FWO, KAS, and Starink	69.38, 69.87, and 67.25	Nucleation and diffusion	[198]
Barley straw	NaOH	Alkali (Basic)	Friedman	138.02	Nucleation and Vasudev (V2)	[16]
Bamboo	ZSM-5	Acidic	Friedman	114.82	Nucleation (A4)	[22]
Red algae	KOH	Alkali (Basic)	Friedman	116.85	Vasudev (V2)	[22]
Chlorella sp.	Ni/θ-Al_2O_3	Supported metal	Friedman and KAS	186.29 and 166.81	-	[199]
Chlorella vulgaris	HZSM-5	Acidic	FWO, KAS, Starink, and Vyazovkin	145.26, 147.84, 145.55, and 145.59	-	[193]
MSW	Al-SBA-15	Acidic	Friedman	86	Diffusion	[102]
Waste fishing nets	ZSM-5	Acidic	KAS, FWO, Friedman, Vyazovkin, and Cai	151.40, 185.90, 200.80, 158.25, and 161.15	-	[200]
Chitin	Calcined dolomite	Metal oxide	C-R and Friedman	138.43 and 124.88	-	[201]
Bamboo	N-doped biochar	Doped carbon material	KAS, Friedman, Starink, and Kissinger	168.46, 166.30, 169.35, and 164.17	Chemical, diffusion, and nucleation	[202]

Table 6. Synergistic effects during co-pyrolysis of mixed feedstocks.

Feedstock	Catalyst	Synergistic Metric	Quantitative Value	Reference
Soyabean husk and HDPE	HZSM-5	Reduced activation energy and enhanced hydrocarbon yields	Waste to catalyst ratio (1:1 to 1:5) reduced activation energy by 30% and increased H-C production by 25%.	[203]
Sugarcane bagasse and HDPE	-	Higher liquid yields	Oil with 34% higher carbon content, 47% higher hydrogen content, and 70% lower oxygen content compared to sugarcane bagasse pyrolysis.	[204]
Enteromorpha prolifera and HDPE	HZSM-5	Reduced amount of acid, oxygenated compounds, and nitrogen compounds in oil	Increased heating value from 30.644 MJ/kg to 42.01 MJ/kg, reduced acids from 13.1% to 7.68% (acetic acid), pyridine, 3-methyl from 5.43% to 2.14%.	[181]
Fir, Chestnut, PE, and PS	-	Increased H/C ratio and decreased O/C ratio	Maximum synergistic effects were observed with 30% plastic.	[205]
Cherry seed and polyvinyl chloride	-	Decrease in activation energy of biomass pyrolysis	Activation energy decreased from 268.5 kJ/mol (cherry seed) to 167.8 kJ/mol with a mixing ration of 1:1.	[206]
Date palm waste and PE foam	-	Reduced activation energy of plastic pyrolysis	A reduction from 216.33 kJ/mol to 206.47 kJ/mol was observed.	[207]
Waste office paper and HDPE	-	Reduced activation energy	Highest decrease in activation energy from 262.3 to 209.3kJ/mol was observed at mixing ratio of 2:1.	[208]
Coffee grains and PE	-	Reduced activation energy	Reduced activation energy (268.32–218.58 kJ/mol) with mixing ratio 7:3.	[209]

4.4. Impact of Catalyst and Reactor Environment

While fundamental models like random and end-chain scission describe initial polymer breakdown or biomass component decomposition, the apparent kinetics in catalytic pyrolysis are devastatingly shaped by the interaction of primary volatiles with catalyst and reactor environment. Three dominating, but often overlooked factors are catalyst pore confinement, secondary vapor phase reactions, and coke formation and dynamic deactivation.

Catalyst pore confinement in microporous/mesoporous materials (e.g., zeolites, MCM-41) imposes steric and diffusion constraints, increasing intermediate residence time, enabling shape-selective aromatization, and masking intrinsic kinetics with mass transfer resistances, yielding higher apparent activation energies [26,210]. Primary pyrolysis vapors undergo extensive secondary cracking, oligomerization, deoxygenation, and aromatization over acid sites, making product selectivity dependent on these sequential reactions rather than primary scission alone [211,212]. Continuous coke deposition progressively blocks sites and pores, altering activity and selectivity with time-on-stream (TOS) and causing lab-to-reactor performance gaps when deactivation is ignored [213]. Predictive kinetic models for catalytic pyrolysis thus require multi-scale frameworks integrating intrinsic kinetics, diffusion modules, secondary reaction networks, and time-dependent deactivation functions to accurately link fundamental mechanisms to apparent kinetics [214].

5. Advanced Modelling Approaches and Deactivation Kinetics

Advanced kinetic modelling approaches used for catalytic pyrolysis are performed through computational frameworks. Even though, a valuable correlation between reaction rates and operation variables is well understood through modeling techniques discussed above, but they have limitations of not considering molecular-level resolution or catalyst lifespan prediction. Now, critical kinetic modelling domains such as microkinetic modelling, process simulation by integrating lumped systems, and catalyst deactivation are explored in this section. These advanced approaches formulate a multi-scale framework by addressing limitations of conventional kinetic analysis methods.

5.1. Microkinetic Modelling and Density Functional Theory Insights

The most granular method of kinetic analysis during catalytic pyrolysis is microkinetic modelling, which describes every elementary step through reaction networks [215]. It takes into consideration the surface intermediate concentration and active site structures. This approach is particularly important for catalytic pyrolysis involving a series of complex reactions [216]. Further, it can integrate the density functional theory (DFT) to determine thermokinetic parameters without any experimental fitting. DFT uses Schrodinger equation to provide catalyst and adsorbate structures for predicting activation barriers and reaction energy for every step involved in the reaction [217]. DFT calculations during catalytic pyrolysis using acid catalysts explained the carbocation formation, deoxygenation pathways, and aromatization mechanisms. Particularly, strong reliance of activation

energy values over carbocation intermediates is measured through proton transfer from acid sites to oxygenated compounds or olefins [218]. In addition, deoxygenation pathways predict the comparative energy barriers for dehydration, decarboxylation, and decarbonylation reactions. Further, conversion of linear intermediates into aromatics is governed via step-wise cyclization and dehydrogenation during DFT calculations [219]. Besides, microkinetic modelling shows enhanced performance when DFT is linked with experimental data for kinetic analysis. For this, mechanistic validation of reaction networks proposed is performed with experimental distribution of product yields. Later on, active site characterization is performed to relate the activation energies with density and strength of active sites. It also allows to identify the relationship between catalyst properties to guide for design of catalyst [220,221].

5.2. Process-Scale Simulation and Lumped Kinetic Models

Process-scale simulations provide a deep understanding for reactor design, techno-economic analysis, and energy integration thorough kinetic modeling for catalytic pyrolysis processes. Typical execution of the process scale simulations comprises primarily the reactor module selection, method definition to select suitable thermodynamic packages, and employment of kinetic parameters from lumped models [222]. Further, this advanced process simulation deals with various complexities of catalytic pyrolysis kinetics by providing the molecular scale insights from microkinetic modelling and DFT calculations to evaluate reactions pathways and their sensitivity towards process conditions [223]. Also, lumped kinetic systems describe both reaction rates as well the product yields. It combines kinetic models to mass and energy balance, separation units, and heat exchanger networks for process optimization. This technique is important to determine the optimum catalyst to feedstock ratio for balanced reaction rates [224]. However, execution of catalytic pyrolysis kinetics in process simulators undergo several challenges such as feedstock variability, catalyst deactivation, and heat integration complexity. Because most of the kinetic models consider that the catalytic activity remains uniform or constant throughout the process and neglect the decay of catalyst with time. Also, coupling to pyrolysis endothermic nature with exothermic nature of catalyst affect the kinetic parameters [225]. Despite this, process-scale simulations are important tools for understanding the reaction kinetics for industrial applications. For instance, parameters from DAEM obtained via TGA have been implemented in Aspen Plus reactor models to predict product yields. Also, it becomes important to explore the catalyst deactivation kinetics.

Therefore, to address this gap between laboratory-derived kinetics and process-scale simulations, real-life applications demonstrate the integration workflow, where parameters from DAEM obtained using TGA are employed in Aspen Plus reactor models to forecast the product yields. Improved chemical kinetics simulations were incorporated in Aspen Plus for lignocellulosic biomass pyrolysis, using RYIELD reactors and pseudo-components to represent volatiles and obtained a good agreement with pilot-scale data through adjustments for heat transfer and yield correlations [226]. For CFD modeling of fluidized-bed catalytic pyrolysis reactors, detailed reaction kinetics were simplified into a lumped four-step scheme (heavy oil→ gasoline→ light gases→ coke), derived from catalytic cracking mechanisms. This scheme was integrated into Eulerian-Eulerian CFD frameworks to simulate reactor hydrodynamics and predict product selectivity. The models also included the effectiveness factors to account for deactivation and secondary reactions [227]. Such workflows demonstrate that the integration of lumped kinetic schemes requiring careful species lumping and scaling factor adjustments, ensures mass and energy balance closure, maintaining computational feasibility while capturing key pathways for reactor-scale predictions. Despite this, a critical parameter tuning is required for direct transfer of experimental kinetics to simulators. The compensation effects between E and A can lead to rate mispredictions under reactor-scale conditions [111]. Also, the lab-scale kinetics studies often neglect the scale-dependent phenomena such as heat and mass transfer limitations, in-situ catalyst deactivation from coke, and secondary reactions [228]. Further, lumping also contribute in gathering the detailed spectra into broad categories and losing selectivity details, which requires stoichiometric tuning against plant data and limiting extrapolation [214]. Consequently, addressing these challenges encompasses the personalized approaches based on source of data and type of simulator. For TGA-derived DAEM in Aspen Plus lumped models, transport omissions and high-rate overpredictions are mitigated by pre-exponential scaling or pseudo-component additions [229]. For the detailed micro kinetics in CFD fluidized beds, over-lumping and deactivation are handled using the reduced lump schemes and supporting hybrid methods [230], while the lab-scale fixed-bed global rates scaled to process simulators need careful tuning of Thiele modulus for transport governance [231]. Eventually, the hybrid kinetic-transport modeling with calibration improves the consistency of scale-up processes for catalytic pyrolysis.

5.3. Catalyst Deactivation Kinetics

Catalytic pyrolysis is largely affected by the deactivation of catalyst in form of coking or coke deposition, sintering, poisoning, and mechanical attrition mechanisms [232]. Particularly, active sites are blocked from deposition of carbonaceous materials, condensation of aromatic compounds, and olefinic polymerization, while loss of active surface area occurs from decay of catalyst structure results into sintering. Further, biomass ash contaminants (i.e., Na, K, and Ca) and plastic waste impurities (i.e., N, S, Cl) lead to poisoning of catalyst [233]. Also, fluidized bed systems result into breakdown of catalyst particles through mechanical attrition.

Deactivation kinetics is modeled through time-on-stream (TOS) models, which provide a practical framework to quantify the catalyst deactivation [234]. Commonly TOS include separable kinetics and site-coverage models. Separable kinetics express the overall reaction rate (r) as the function of initial rate (r_0) and deactivation function [235]. This can be expressed through following expression:

$$r(t) = r_0 \times a(t) \tag{10}$$

Here, a(t) represents the activity function for catalyst decays with TOS.

Further, site-coverage models consider the fraction of active sites that are blocked or covered by coke [236]. It is expressed in the following form:

$$-\frac{\mathrm{d}\theta_c}{\mathrm{d}t} = -k_\mathrm{d}(1-\theta_c)^n \tag{11}$$

Here, θ_c denotes the fraction of deactivated sites, while k_d represents the deactivation rate constant. It is important to mention that second order decay model is generally followed during catalyst deactivation kinetics as coke formation shows the bimolecular nature [237].

Recent studies provide quantitative insights into deactivation parameters across different systems. For instance, in CO_2 methanation over Ni/Al_2O_3, hydrothermal sintering and CO-induced restructuring increased the apparent activation energy from 141.6 kJ/mol to 200.4 kJ/mol, corresponding to significant activity loss under optimal conditions [238]. Similarly, a modified Weibull distribution model for a Cu-based catalyst in formaldehyde ethynylation yielded a deactivation energy of 45.8 kJ/mol, a pre-exponential factor of 1.2×10^7 h^{-1}, and first-order deactivation kinetics [239]. Advanced models, such as three stage deactivation frameworks for residual hydrotreating (accounting for active-site formation, coke coverage, and metal deposition) have successfully predicted complex, non-S-shaped deactivation profiles and product properties [240]. These examples highlight the quantitative application of deactivation models, yielding specific kinetic parameters that describe the rate and extent of activity loss.

Additionally, a critical challenge remains in experimental validation of these models under realistic, long duration pyrolysis conditions. Most quantitative studies derive parameters from controlled, short-duration experiments [241,242]. While valuable for parametrizing models, such data may not capture prolonged deactivation mechanisms (i.e., slow sintering, pre blockage) that dominate the continuous industrial operation. Among the models, separable kinetics (TOS) models are often validated against bench scale runs of several hours [235,238], whereas structure-based models require advanced operando characterization rarely applied in pyrolysis studies [241,242]. Consequently, the reliability of deactivation kinetics for predictive scale-up is constrained by a scarcity of long-term, high-resolution kinetic data collected under relevant process conditions. Future work must prioritize long-term deactivation experiments coupled with operando characterization to correlate activity loss with specific structural changes, transforming these models from descriptive tools into predictive assets for reactor design.

Furthermore, deactivation kinetics is also approached through structure-based model, multi-mechanism models, and deactivation mapping. These structure-based models interpret pore structure evolution of catalyst during deactivation to identify coke deposition over micropores, which affects the effectiveness of internal diffusion [241]. Subsequently, multi-mechanism models combine the multiple deactivation pathways viz. sintering and coking during kinetic modelling [242]. Deactivation mapping approach tend to create operational diagrams to identify deactivation regimes to allow positive moderation tactics. Figure 10 shows the mechanism and modelling of deactivation of catalyst.

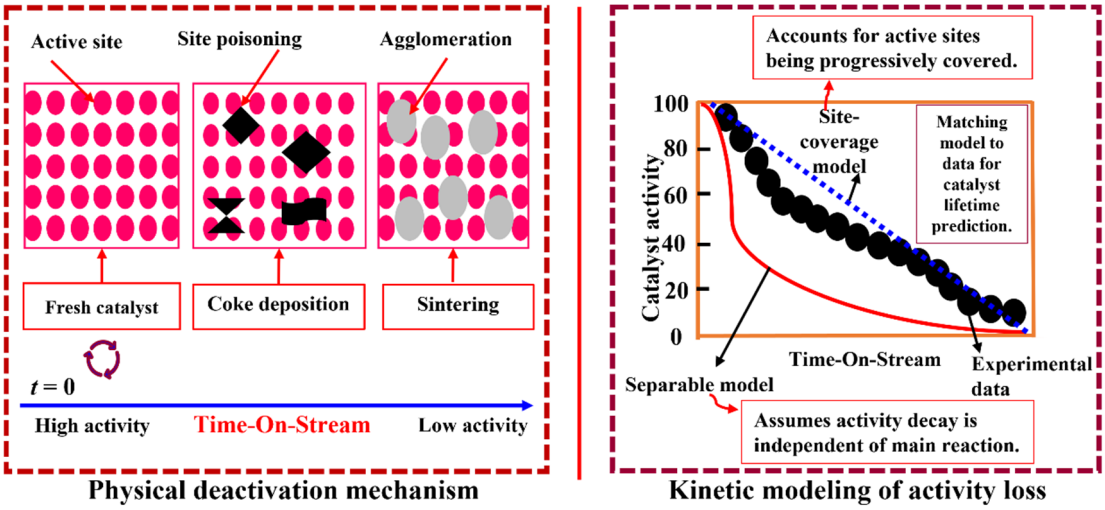

Figure 10. Mechanism and modeling of catalyst deactivation [243].

6. Challenges in Catalytic Pyrolysis

6.1. Feedstock Variability and Data Discrepancy

Despite the reassuring developments in catalytic pyrolysis, a number of challenges still remain unanswered. The development of robust kinetic models faces primary challenges due to feedstock variability and inherent characteristics during catalytic pyrolysis. For instance, model compounds (i.e., xylan, PE, cellulose) can help to examine the reaction pathways but cannot evaluate the inhibitory and synergistic effects. Similarly, MSW can create a very complex reactive environment due to its heterogeneous nature, it leads to significant changes in E values as well as the reaction mechanisms as compared to real or pure feedstocks. However, these challenges provide a thoughtful practical inference by often providing very poor predictions from model compounds for industrial feedstocks. This problem requires the advancement of composition-adaptive kinetic models which can consider feedstock variability as well its effect over reaction mechanisms and reaction rates.

Further, kinetic parameters are also influenced by various sources such as reactor configuration, experimental protocol, and analytical methods employed. For example, experimental data measured through various reactors such as fixed-bed, TGA, and fluidized bed, carry several heat and mass transfer characteristics, yielding discrepancy in kinetic parameters. Also, variation in catalytic loadings, feedstock particle size, and heating rates affect the reaction kinetics. Therefore, to establish the reliable kinetic analysis database, standardized conventions need to be followed alongside conducting comparative revisions.

6.2. Heat and Mass Transfer Limitations

Another hurdle that lies in progress of catalytic pyrolysis kinetics is the disparity between intrinsic and apparent kinetics, since the combined physical and chemical processes are reflected during experimental measurement of global reaction rates. It includes various limitations such as intra-particle diffusion, inter-phase heat transfer, and boundary layer effects. These limitations can lead to underestimation of activation energies and wrong reaction order from complicated inherent chemical kinetics. Also, the change from chemical to diffusion reaction control during catalytic pyrolysis affects understanding of kinetic triplet directly. Further, these transport phenomena are affected by deactivation of catalyst in form of coke deposition which alters the accessibility of active sites and structure of pores. So, catalyst deactivation is another challenge which needs to be addressed.

6.3. Catalyst Deactivation

One of the most poorly quantified aspects during the kinetic analysis of catalytic pyrolysis is the catalyst deactivation. Its complexity arises from the loss of catalytic activity of catalysts with time that requires inclusion of an extra parameter (TOS) which is often not considered in the conventional kinetic analysis techniques. Also, literature have vastly reported the kinetic triplets using fresh catalysts. This leaves a very big gap in progress of lab-scale to industrial scale measurements where catalysts are employed regularly without considering their deactivation with time. Further, deactivation also occurs through various simultaneous mechanisms such as coking, sintering, and poisoning. These simultaneous deactivation mechanisms also complicate the kinetics. Therefore, it

is required to decouple and quantify these mechanisms and their contributions in overall activity loss during development of predictive models for catalyst deactivation kinetics.

7. Knowledge Gaps and Future Perspectives

7.1. Knowledge Gaps

The absence of standard kinetics protocols for catalytic pyrolysis is the most critical gap. Also, catalytic pyrolysis lacks in various aspects such as method validation using standard reference, protocol specifications for reactor types as well as kinetic modelling to associate the uncertainties. This gap obstructs the direct association of results presented in various studies with slowly progressing kinetic models. Further, a clear knowledge gap lies in understanding of in-situ and ex-situ configurations for the comparison of reaction rates and pathways, understanding of product distribution kinetics from volatile and catalyst contact duration, and modelling the kinetics consequences of heat transfer limitations. Additionally, kinetics implications arise from the catalyst-adsorbent interaction in the initial stages. However, DFT calculations consider the ideal surface interactions, but they neglect the multicomponent and complex nature of pyrolysis vapors. It is important to consider the adsorption interaction, surface residence time and its effect over reaction pathways, and accessibility of catalytic active sites during kinetic modelling for the catalytic pyrolysis.

7.2. Future Perspectives

Further researches are required to integrate advanced methodologies for overcoming the existing challenges. Use of in-situ and operando characterization approaches like Raman and X-ray absorption spectroscopy (XAS) can directly observe the catalyst behavior alongside simultaneous measurement of kinetic triplets. It is also important for analyzing the catalysts-adsorbate interactions and catalyst deactivation processes. Subsequently, kinetic analysis should incorporate the ML and AI to navigate the complexity of feedstock, predict the kinetic triplet, and optimize the process conditions. This will prioritize the advancement of multi-scale models to connect molecular-level phenomena with process-scale simulation. Lastly, the kinetic studies should also consider the properties of emerging catalyst systems such as single-atom catalyst, engineered biochar, and hierarchical zeolites. These emerging catalysts display dissimilar kinetic behavior which cannot be defined effectively using the conventional kinetic methods employed for the traditional catalysts. Therefore, it will be important to understand kinetics of these next-generation catalytic resources to harness their full potential.

7.2.1. Industrial Applications and Scale-Up Challenges

While most of the research studies focusing on kinetics are performed for laboratory scale, several new industrial and pilot-scale projects demonstrate the commercial pathway for catalytic pyrolysis, which bridges the gap between real-world operations and fundamental kinetics. For example: catalytic thermochemical pathways are used for full-scale municipal waste to advanced biofuels and chemicals generation facility of Enerkem. Also, catalytic depolymerization was employed for chemical recycling of polystyrene at large scale by Agilyx. Additionally, large-scale fluid-catalytic cracking process is a comparable industrial process for catalytic cracking, providing suggestions on catalyst deactivation consideration and kinetics for large-scale systems. However, it faces several challenges from an industrial viability standpoint. Therefore, it is important to handle the highly variable waste streams to make adaptive kinetic models for real world applications to ensure stable operation. Also, the economics of catalyst management, directly governed by deactivation kinetics is important for the catalyst lifetime, regeneration strategies, and cost-benefit analyses. Most importantly, the robust kinetic models lay foundation for techno-economic assessment (TEA) and life-cycle analysis (LCA), ensuring commercial feasibility. The kinetic parameters provide the important inputs for process simulators to predict the yields, utility demand, reactor size. Subsequently, reliable LCA studies also depend upon the process models to govern the environmental benefits of the technology.

By focusing these future perspectives, catalytic pyrolysis community can progress towards development of robust kinetic models for predictive kinetic modelling of diverse waste feedstocks in a sustainable way for industrial-scale applications.

7.2.2. Implementation Pathways

In order to translate the future perspectives into actionable development, structured implementation pathways are required. A practical pipeline for in-situ and operando characterization involves developing spectroscopy-compatible reactor cells for realistic conditions, synchronizing spectral data with real-time product analysis, and

using innovative algorithms to directly compare the spectral characteristics with kinetic variations. Subsequently, an integration of robust ML/AI involves building curated, open-access kinetic databases and developing hybrid, physics-informed neural networks which are validated for the lab and pilot scale studies. For novel catalysts, a personalized system from controlled synthesis and in-situ analysis to microkinetic modeling that detect unique active-site formations are required. Finally, confirming industrial relevance requires a closed-loop scale-up framework comprising intrinsic kinetics from the optimized lab experiments updating the CFD models of pilot reactors. Further, these models are iteratively refined using operational pilot data and finally used for TEA and LCA to generate a feedback loop where economic aims guide essential research implications.

8. Conclusions

In this review, we have summarized the current state of art knowledge in the field of catalytic pyrolysis kinetics for different waste feedstocks. The inclusion of catalysts generally alters the reaction pathways, indicating decreasing activation energy for several feedstocks, while it also showed enhanced product selectivity in form of cracking, deoxygenation, and aromatization reactions. Also, development of methodologies for model-free and model-fitting isoconversional kinetic analysis methods was explained. In addition, multi-step kinetic models showed enhanced performance in describing the kinetic parameters accurately for real wastes such as municipal solid waste, while machine learning has emerged as a powerful tool to deal with the complexities of these real heterogeneous wastes. Further, varying kinetic behavior of different feedstocks was observed using multi-component decomposition kinetics which was further complicated by mixed-feedstocks posing significant synergistic effects. The development of integrated multi-scale modeling frameworks can integrate DFT with reactor-level simulations to create advanced predictive proficiencies from molecular-scale to process-scale. Still, feedstock variability and complexity, heat and mass transfer limitations, and study of kinetics during deactivation of catalyst pose significant challenges during kinetic modelling for catalytic pyrolysis processes. Addressing these limitations indicate towards the employment of in-situ and operando characterization techniques, predictive machine learning, and study of emerging catalyst systems. Finally, the development of the robust and adaptive kinetic models which consider the variabilities of feedstocks in real world and activity of catalysts with time is crucial to transform catalytic pyrolysis as commercially feasible practice from only a lab-scale practice for the renewable energy generation and sustainable waste utilization.

Author Contributions: S.R.: conceptualization, methodology, visualization, writing—original draft preparation; Y.P.: writing—reviewing and editing, visualization; F.A.: writing—reviewing and editing, visualization; T.A.M.: writing—reviewing and editing, visualization; Y.Z.: conceptualization, supervision, writing—reviewing and editing, validation, supervision. All authors have read and agreed to the published version of the manuscript

Funding: Financial support was provided by the National Natural Science Foundation of China (52476005), and Heilongjiang Provincial Key R&D Program “Unveiling the Leader” Project (Grant No. 2023ZXJ02C04).

Institutional Review Board Statement: Not applicable.

Informed Consent Statement: Not applicable.

Data Availability Statement: Not applicable.

Conflicts of Interest: The authors declare no conflict of interest.

Use of AI and AI-Assisted Technologies: During the preparation of this work, the authors used DeepSeek to refine the language, while EdrawMax tool was used for drawing the schematics. After using these tools, the authors reviewed and edited the content as needed and take full responsibility for the content of the published article.

References

1. Hsiao, C.Y.; Lin, S.L. Thermal Reactions and Byproducts from the Waste-to-Energy Process of Flame Retardant-Containing Wastes-A Review. *Green Energy Fuel Res.* **2025**, *2*, 109–126. https://doi.org/10.53941/gefr.2025.100009.
2. Marwan-Abdelbaset, E.; Lu, X.Y.; Samy-Kamal, M.; et al. From waste to value: Microbial valorization of low-cost renewable resources for hyaluronic acid production. *Waste Manag.* **2026**, *209*, 115179. https://doi.org/10.1016/j.wasman.2025.115179.
3. Ajona, C.; Saravanakumar, A. Analysis of Thermal Properties in Co-Gasification of Municipal Solid Waste and Woody Biomass. *Green Energy Fuel Res.* **2025**, *2*, 139–151. https://doi.org/10.53941/gefr.2025.100011.
4. Melikoglu, M. Waste valorization strategies with inputs for microalgae biorefineries: A global review. *Clean. Water* **2025**, *4*, 100125. https://doi.org/10.1016/j.clwat.2025.100125.
5. Yesil, H.; Tugtas, A.E.; Çalli, B. Beyond landfills: Transforming biodegradable waste into climate solutions and valuable resources. *Rev. Environ. Sci. Bio Technol.* **2025**, *24*, 805–829. https://doi.org/10.1007/s11157-025-09739-1.

6. Fang, Y.; Tang, Y.; Li, G.; et al. Co-pyrolysis of waste biomass and plastics from food packaging waste: Pyrolysis characteristics, synergetic effects, and reaction kinetics. *J. Environ. Manag.* **2025**, *395*, 127800. https://doi.org/10.1016/j.jenvman.2025.127800.
7. Sun, Y.; Deng, J.; Zhang, F.; et al. Global distribution and warming effect of brown carbon from shipping emissions. *Carbon Res.* **2025**, *4*, 44. https://doi.org/10.1007/s44246-025-00212-w.
8. Sun, D.; Zeng, X.; Wang, F.; et al. Gas generation characteristics and kinetics during catalytic pyrolysis of distiller's grains by coal slag for coordinated utilization via gasification. *J. Environ. Manag.* **2025**, *394*, 127388. https://doi.org/10.1016/j.jenvman.2025.127388.
9. Yoon, S.; Lee, Y.; An, H.; et al. Sustainable woody biochar application for improving net ecosystem carbon budget, yield and soil properties in red pepper cropping systems: A two-year field study. *Biochar* **2025**, *7*, 112. https://doi.org/10.1007/s42773-025-00494-8.
10. Ramandani, A.A.; Rachmadona, N.; Munawaroh, H.S.H.; et al. Sustaining Food Waste for Energy Conversion: A Mini Review. *Green Energy Fuel Res.* **2025**, *2*, 34–47. https://doi.org/10.53941/gefr.2025.100004.
11. Vasudev, V.; Ku, X.; Lin, J. Kinetic study and pyrolysis characteristics of algal and lignocellulosic biomasses. *Bioresour. Technol.* **2019**, *288*, 121496. https://doi.org/10.1016/j.biortech.2019.121496.
12. Lee, D.; Nam, H.; Seo, M.W.; et al. Recent progress in the catalytic thermochemical conversion process of biomass for biofuels. *Chem. Eng. J.* **2022** *447*, 137501. https://doi.org/10.1016/j.cej.2022.137501.
13. El-Fawal, E.M.; El-Naggar, A.M.A.; El-Zahhar, A.A.; et al. Biofuel production from waste residuals: Comprehensive insights into biomass conversion technologies and engineered biochar applications. *RSC Adv.* **2025**, *15*, 11942–11974. https://doi.org/10.1039/D5RA00857C.
14. Wang, W.; Gu, Y.; Zhou, C.; et al. Current Challenges and Perspectives for the Catalytic Pyrolysis of Lignocellulosic Biomass to High-Value Products. *Catalysts* **2022**, *12*, 1524. https://doi.org/10.3390/catal12121524.
15. El-Araby, R. Biofuel production: Exploring renewable energy solutions for a greener future. *Biofuels Bioprod. Biorefin.* **2024**, *17*, 129. https://doi.org/10.1186/s13068-024-02571-9.
16. Ram, S.; Ku, X.; Vasudev, V. Catalytic pyrolysis of lignocellulosic and algal biomass using NaOH as a catalyst. *Biofuels Bioprod. Biorefin.* **2024**, *18*, 482–494. https://doi.org/10.1002/bbb.2599.
17. Sulis, D.B.; Lavoine, N.; Sederoff, H.; et al. Advances in lignocellulosic feedstocks for bioenergy and bioproducts. *Nat. Commun.* **2025**, *16*, 1244. https://doi.org/10.1038/s41467-025-56472-y.
18. Nosenzo, S.; Kelman, R. From fields to fuel: Analyzing the global economic and emissions potential of agricultural pellets, informed by a case study. *arXiv* **2025**, arXiv:2508.12457.
19. Loc, N.X.; Phuong, D.T.M. Optimizing biochar production: A review of recent progress in lignocellulosic biomass pyrolysis. *Front. Agric. Sci. Eng.* **2025**, *12*, 148–172. https://doi.org/10.15302/J-FASE-2024597.
20. Ziolkowska, J.R. Biofuels technologies: An overview of feedstocks, processes, and technologies. *Biofuels A More Sustain. Future* **2019**, 1–19. https://doi.org/10.1016/B978-0-12-815581-3.00001-4.
21. Selwal, N.; Sultana, H.; Rahayu, F.; et al. Emerging technologies in biomass conversion: Bioengineering and nanocatalysts to AI-driven process optimization. *Biomass Bioenergy* **2025**, *200*, 108054. https://doi.org/10.1016/j.biombioe.2025.108054.
22. Ram, S.; Ku, X.; Vasudev, V.; et al. Pyrolytic performance and kinetic analysis of non-catalytic and catalytic pyrolysis of bamboo powder and red algae. *Biomass Convers. Biorefin.* **2025**, *15*, 25117–25129. https://doi.org/10.1007/s13399-025-06810-3.
23. Ram, S.; Yadav, S.K.; Yadav, A.; et al. Recent Advancements in Thermochemical Conversion of Biomass and Technologies Used to Eliminate the Tar Formation. In *Biennial International Conference on Future Learning Aspects of Mechanical Engineering*; Springer Nature Singapore: Singapore, 2023; pp. 585–599. https://doi.org/10.1007/978-981-99-2382-3_49.
24. Wei, F.; Sang, S.; Liu, S.; et al. BECCS carbon-negative technologies based on biomass thermochemical conversion: A review of critical pathways and research advances. *Fuel* **2025**, *390*, 134743. https://doi.org/10.1016/j.fuel.2025.134743.
25. Martínez, J.D.; Puy, N.; Murillo, R.; et al. Waste tyre pyrolysis—A review. *Renew. Sustain. Energy Rev.* **2013**, *23*, 179–213. https://doi.org/10.1016/j.rser.2013.02.038.
26. Rahman, M.M.; Liu, R.; Cai, J. Catalytic fast pyrolysis of biomass over zeolites for high quality bio-oil—A review. *Fuel Process. Technol.* **2018**, *180*, 32–46. https://doi.org/10.1016/j.fuproc.2018.08.002.
27. Patlolla, S.R.; Katsu, K.; Sharafian, A.; et al. A review of methane pyrolysis technologies for hydrogen production. *Renew. Sustain. Energy Rev.* **2023**, *181*, 113323. https://doi.org/10.1016/j.rser.2023.113323.
28. Chanda, M. Chemical aspects of polymer recycling. *Adv. Ind. Eng. Polym. Res.* **2021**, *4*, 133–150. https://doi.org/10.1016/j.aiepr.2021.06.002.
29. Chen, Z.; Wei, W.; Chen, X.; et al. Upcycling of plastic wastes for hydrogen production: Advances and perspectives. *Renew. Sustain. Energy Rev.* **2024**, *195*, 114333. https://doi.org/10.1016/j.rser.2024.114333.

30. Shoaib, M.; Ku, X.; Ram, S. Thermogravimetric characteristics and product distribution behavior during co-pyrolysis of Datong coal with two different biomasses. *Int. J. Coal Prep. Util.* **2025**, 1–16. https://doi.org/10.1080/19392699.2025.2563811.
31. Aysu, T.; Durak, H. Catalytic pyrolysis of liquorice (*Glycyrrhiza glabra* L.) in a fixed-bed reactor: Effects of pyrolysis parameters on product yields and character. *J. Anal. Appl. Pyrolysis* **2015**, *111*, 156–172. https://doi.org/10.1016/j.jaap.2014.11.017.
32. Ismail, T.M.; Banks, S.W.; Yang, Y.; et al. Coal and biomass co-pyrolysis in a fluidized-bed reactor: Numerical assessment of fuel type and blending conditions. *Fuel* **2020**, *275*, 118004. https://doi.org/10.1016/j.fuel.2020.118004.
33. Wu, Y.; Wang, H.; Li, H.; et al. Applications of catalysts in thermochemical conversion of biomass (pyrolysis, hydrothermal liquefaction and gasification): A critical review. *Renew. Energy* **2022**, *196*, 462–481. https://doi.org/10.1016/j.renene.2022.07.031.
34. Yani, A.; Wijayanti, W.; Sasongko, M.N.; et al. Synergistic co-pyrolysis of polyethylene terephthalate and *Hibiscus rosa-sinensis*: Catalytic mechanisms for optimizing pyrolysis yields. *South Afr. J. Chem. Eng.* **2025**, *53*, 281–302. https://doi.org/10.1016/j.sajce.2025.05.008.
35. He, Q.; Wang, Q.; Luan, J. A review on biomass pyrolysis and pyrolysis mechanisms. *Biofuels* **2025**, 1–21. https://doi.org/10.1080/17597269.2025.2537515.
36. Kim, J.Y.; Yoo, Y.; Lee, D.J.; et al. Catalytic pyrolysis of three industrial fungal biomass to enhance syngas production. *Fuel* **2026**, *405*, 136748. https://doi.org/10.1016/j.fuel.2025.136748.
37. Tahir, M.H.; Ali, A.; Vasudev, V. Enhancing monocyclic aromatics hydrocarbons production via catalytic co-pyrolysis of cabbage biomass and low-density polyethylene with ZnO/ZSM-5 catalyst. *J. Anal. Appl. Pyrolysis* **2026**, *193*, 107391. https://doi.org/10.1016/j.jaap.2025.107391.
38. Raj, A.; Ghodke, P.K. Investigation of in situ and ex situ catalytic pyrolysis of lignocellulosic biomass waste for the production of de-oxygenated C8–C18 range enhanced liquid fuel precursor—reaction mechanisms and optimization. *J. Anal. Appl. Pyrolysis* **2025**, *191*, 107179. https://doi.org/10.1016/j.jaap.2025.107179.
39. Xie, K.; Liu, Z.; Zhang, M.; et al. Understanding the Transient Microwave Drying Performances of Industrial Sewage Sludge Towards Green Fuel and Energy. *Green Energy Fuel Res.* **2025**, *2*, 174–186. https://doi.org/10.53941/gefr.2025.100013.
40. Zhao, W.; Cao, W.; Cui, L.; et al. Energy and Exergy Performances of Corn Straw and SiC during the Microwave Heating Process. *J. Therm. Sci.* **2025**, *34*, 1857–1866. https://doi.org/10.1007/s11630-025-2173-7.
41. Ke, L.; Zhou, N.; Wu, Q.; et al. Microwave catalytic pyrolysis of biomass: A review focusing on absorbents and catalysts. *NPJ Mater. Sustain.* **2024**, *2*, 24. https://doi.org/10.1038/s44296-024-00027-7.
42. Wei, S.; Zhou, T.; Yang, D.; et al. Microwave-induced and catalytic pyrolysis of municipal domestic waste under multiple synergistic effects. *J. Renew. Sustain. Energy* **2025**, *17*, 023101. https://doi.org/10.1063/5.0250134.
43. Tiwari, M.; Vinu, R. In situ and ex situ catalytic microwave pyrolysis of biomass pellets using Ni/Al_2O_3 for hydrogen and bio-oil production. *J. Anal. Appl. Pyrolysis* **2025**, *189*, 107044. https://doi.org/10.1016/j.jaap.2025.107044.
44. Yang, X.; Yu, J.; Zeng, M.; et al. Complete valorization of lignocellulosic biomass through integrated reductive catalytic fractionation and microwave-assisted pyrolysis. *J. Anal. Appl. Pyrolysis* **2025**, *188*, 107049. https://doi.org/10.1016/j.jaap.2025.107049.
45. Shi, X.; Wang, B.; Hu, J.; et al. Investigating the synergistic driving action of microwave and char-based multi-catalysts on biomass catalytic pyrolysis into value-added bio-products. *Renew. Energy* **2023**, *219*, 119490. https://doi.org/10.1016/j.renene.2023.119490.
46. He, M.; Zhao, J.; Wang, D.; et al. Microwave-assisted catalytic pyrolysis of biomass with biochar materials derived from spent lithium-ion batteries: Microwave absorption and pyrolysis characteristics. *J. Environ. Chem. Eng.* **2024**, *12*, 112099. https://doi.org/10.1016/j.jece.2024.112099.
47. Sharma, S.; Tsai, M.L.; Sharma, V.; et al. Environment Friendly Pretreatment Approaches for the Bioconversion of Lignocellulosic Biomass into Biofuels and Value-Added Products. *Environments* **2023**, *10*, 6. https://doi.org/10.3390/environments10010006.
48. Vuppaladadiyam, A.K.; Vuppaladadiyam, S.S.V.; Awasthi, A.; et al. Biomass pyrolysis: A review on recent advancements and green hydrogen production. *Bioresour. Technol.* **2022**, *364*, 128087. https://doi.org/10.1016/j.biortech.2022.128087.
49. Zhang, J.; Zhang, B.; Xia, A.; et al. Production of carbon dots, biofuels, bio-adsorbents, and biological nutrients via hydrothermal conversion of *Chlorella pyrenoidosa* and oilseed rape straw. *Biochar* **2025**, *7*, 109. https://doi.org/10.1007/s42773-025-00482-y.
50. Du, K.; Zhong, W.; Chen, X.; et al. Co-Pyrolysis of Coal and Waste Plastic: Characterization and Rapid Tar Yield Prediction Method. *J. Therm. Sci.* **2025**, *34*, 1599–1611. https://doi.org/10.1007/s11630-025-2174-6.
51. Islam, K.M.O.; Ahmad, N.; Ummer, A.C.; et al. Microwave-Assisted pyrolysis of waste plastics: A comprehensive review on process parameters, catalysts, and future prospects. *Results Eng.* **2025**, *26*, 105571. https://doi.org/10.1016/j.rineng.2025.105571.

52. Yuan, J.; Yang, G.; Zhou, X.; et al. Functional carbon materials from waste plastics: Synthesis and applications. *Sustain. Carbon Mater.* **2025**, *1*, e002. https://doi.org/10.48130/scm-0025-0005.
53. Huang, C.; Tang, C.; Liu, J.; et al. Insight into the catalytic role of industrial solid waste in improving gas quality during biomass pyrolysis. *Carbon Resour. Convers.* **2025**, 100339. https://doi.org/10.1016/j.crcon.2025.100339.
54. Zhu, Z.; Zhou, Z.; Zhang, Z.; et al. Analysis of municipal solid waste (MSW) pyrolysis products using synchrotron vacuum ultraviolet photoionization mass spectrometry: Effects of CaO and NH_3. *J. Anal. Appl. Pyrolysis* **2026**, *193*, 107441. https://doi.org/10.1016/j.jaap.2025.107441.
55. Murphy, F.; Gusciute, E.; Mediboyina, K.; et al. *Social and Environmental Sustainability of Municipal Solid Waste in the Context of the UN Sustainable Development Goals*; IEA Bioenergy: Ottawa, ON, Canada, 2025.
56. Suriapparao, D.V.; Sridevi, V.; Ramesh, P.; et al. Synthesis of sustainable chemicals from waste tea powder and Polystyrene via Microwave-Assisted in-situ catalytic Co-Pyrolysis: Analysis of pyrolysis using experimental and modeling approaches. *Bioresour. Technol.* **2022**, *362*, 127813. https://doi.org/10.1016/j.biortech.2022.127813.
57. Bakhtiar, M.; Shahbaz, M.; Ayub, H.M.U.; et al. Steam gasification of plastic and woody biomass for hydrogen-rich syngas production with CO_2 reduction, emission and energy analysis. *Energy* **2025**, *334*, 137718. https://doi.org/10.1016/j.energy.2025.137718.
58. Liu, M.; Dong, W.; Ni, H.; et al. Co-pyrolysis of sea rice straw and low-density polypropylene: Implications for advancing sustainable fuel production. *J. Anal. Appl. Pyrolysis* **2025**, *192*, 107283. https://doi.org/10.1016/j.jaap.2025.107283.
59. Li, X.; Chen, X.; Zhang, C.; et al. PM_{10} emissions from co-combustion of water washed sea rice waste with coal. *Appl. Energy* **2024**, *356*, 122446. https://doi.org/10.1016/j.apenergy.2023.122446.
60. Sathish, T.; Ammar, M.B.; Sabeur, H.; et al. Hydrogen production from greywater algae biomass via Pyrolysis: Influence of temperature and polyaniline integrated sodium hydroxide (PANI-NaOH) catalyst. *Case Stud. Therm. Eng.* **2025**, *73*, 106639. https://doi.org/10.1016/j.csite.2025.106639.
61. Ong, M.Y.; Milano, J.; Nomanbhay, S.; et al. Insights into algae-plastic pyrolysis: Thermogravimetric and kinetic approaches for renewable energy. *Energy* **2025**, *314*, 134322. https://doi.org/10.1016/j.energy.2024.134322.
62. Zhao, Z.; Tian, H.; Chen, Z.; et al. Upgrading of bio-oil from torrefied wheat straw over Fe-Ni modified HZSM-5@MCM-41: Influence of pyrolysis temperature and catalyst-feedstock ratio. *J. Energy Inst.* **2026**, *124*, 102366. https://doi.org/10.1016/j.joei.2025.102366.
63. Patil, Y.; Ku, X. Pyrolysis kinetics and thermodynamic behavior of pseudo components of raw and torrefied maple wood. *Energy Sources Part A* **2024**, *46*, 462–474. https://doi.org/10.1080/15567036.2023.2285406.
64. State, R.N.; Ionescu, G.; Volceanov, A.; et al. Combined valorization of bone waste as feedstock and support material for ex-situ catalytic pyrolysis. *J. Environ. Chem. Eng.* **2025**, *13*, 119091. https://doi.org/10.1016/j.jece.2025.119091.
65. Patil, Y.; Ku, X. Comparison and characterization of torrefaction performance and pyrolysis behaviour of softwood and hardwood. *Energy Sources Part A* **2022**, *44*, 8860–8877. https://doi.org/10.1080/15567036.2022.2126561.
66. Isahak, W.N.R.W.; Al-Amiery, A. Catalysts driving efficiency and innovation in thermal reactions: A comprehensive review. *Green Technol. Sustain.* **2024**, *2*, 100078. https://doi.org/10.1016/j.grets.2024.100078.
67. Hussain, A.; Ghaffar, I.; Sattar, S.; et al. Eco-friendly Catalysts Revolutionizing Energy and Environmental Applications: An Overview. *Top. Catal.* **2025**, *68*, 487–509. https://doi.org/10.1007/s11244-024-01976-y.
68. Shanthini, V.S.; Chitra, D.; Moorthy, G. Biodiesel: A comprehensive review of properties, catalyst types, and feedstock sources. *Results Chem.* **2025**, *18*, 102678. https://doi.org/10.1016/j.rechem.2025.102678.
69. Kojima, T. Chapter 1 Overview of the Catalytic Chemistry of Metal Complexes. *R. Soc. Chem.* **2024**, *2*, 1–7. https://doi.org/10.1039/9781837676484-00001.
70. Mirshafiee, F.; Khoshbin, R.; Karimzadeh, R. A green approach for template free synthesis of Beta zeolite incorporated in ZSM-5 zeolite to enhance catalytic activity in MTG reaction: Effect of seed nature and temperature. *J. Clean. Prod.* **2022**, *361*, 132159. https://doi.org/10.1016/j.jclepro.2022.132159.
71. Yoshimura, T.; Tanaka, S.; Matsuda, N.; et al. Estimation of catalytic cracking of vacuum gas oil by ZSM-5- and β-zeolite-containing two-layered and novel three-layered hierarchical catalysts using Curie point pyrolyzer. *J. Anal. Appl. Pyrolysis* **2024**, *182*, 106621. https://doi.org/10.1016/j.jaap.2024.106621.
72. Pacheco, J.G.A.; Padilha, J.F.; Santos, B.L.; et al. Hydrogen-free deoxygenation of oleic acid on acidic and basic ZSM-5 and Y-zeolites: Products for biofuel and reaction pathways. *Catal. Today* **2025**, *445*, 115094. https://doi.org/10.1016/j.cattod.2024.115094.
73. Li, H.; Zhang, Z.; Hu, J.; et al. Revealing the mechanisms of biomass fast pyrolysis catalyzed by CaO-modified red mud. *J. Anal. Appl. Pyrolysis* **2026**, *193*, 107444. https://doi.org/10.1016/j.jaap.2025.107444.
74. Keller, M.H.; Moreira, R.; de Bona, J.; et al. Covalent triazine frameworks with MgO sites as a basic catalyst for aldol condensation and transesterification reactions. *Appl. Catal. A Gen.* **2025**, *708*, 120583. https://doi.org/10.1016/j.apcata.2025.120583.

75. Cao, Z.; Niu, J.; Gu, Y.; et al. Catalytic pyrolysis of rice straw: Screening of various metal salts, metal basic oxide, acidic metal oxide and zeolite catalyst on products yield and characterization. *J. Clean. Prod.* **2020**, *269*, 122079. https://doi.org/10.1016/j.jclepro.2020.122079.
76. Zhang, Z.; Zhang, X.; Zhang, L.; et al. Steam reforming of guaiacol over Ni/SiO_2 catalyst modified with basic oxides: Impacts of alkalinity on properties of coke. *Energy Convers. Manag.* **2020**, *205*, 112301. https://doi.org/10.1016/j.enconman.2019.112301.
77. Memarian, Z.; Meshkani, F. CO_2 reforming of glycerol on Ni/Al_2O_3 catalyst: Influence of doping of alkaline earth metals (Mg, Ca, Sr, and Ba) to support. *Biomass Bioenergy* **2025**, *193*, 107578. https://doi.org/10.1016/j.biombioe.2024.107578.
78. Zhang, Z.; Yu, M.; Shen, M.; et al. Promoting effect of alkaline earth metals on Ni/CeO_2 catalysts for ammonia decomposition reaction. *Mol. Catal.* **2025**, *578*, 115016. https://doi.org/10.1016/j.mcat.2025.115016.
79. Hemberger, P.; Custodis, V.B.F.; Bodi, A.; et al. Understanding the mechanism of catalytic fast pyrolysis by unveiling reactive intermediates in heterogeneous catalysis. *Nat. Commun.* **2017**, *8*, 15946. https://doi.org/10.1038/ncomms15946.
80. Chaihad, N.; Karnjanakom, S.; Abudula, A.; et al. Zeolite-based cracking catalysts for bio-oil upgrading: A critical review. *Resour. Chem. Mater.* **2022**, *1*, 167–183. https://doi.org/10.1016/j.recm.2022.03.002.
81. Ye, R.; Ding, J.; Reina, T.R.; et al. Design of catalysts for selective CO_2 hydrogenation. *Nat. Synth.* **2025**, *4*, 288–302. https://doi.org/10.1038/s44160-025-00747-1.
82. Wang, G.; Dai, Y.; Yang, H.; et al. A review of recent advances in biomass pyrolysis. *Energy Fuels* **2020**, *34*, 15557–15578. https://doi.org/10.1021/acs.energyfuels.0c03107.
83. Vuppaladadiyam, A.K.; Vuppaladadiyam, S.S.V.; Sikarwar, V.S.; et al. A critical review on biomass pyrolysis: Reaction mechanisms, process modeling and potential challenges. *J. Energy Inst.* **2023**, *108*, 101236. https://doi.org/10.1016/j.joei.2023.101236.
84. Wang, S.; Dai, G.; Yang, H.; et al. Lignocellulosic biomass pyrolysis mechanism: A state-of-the-art review. *Prog. Energy Combust. Sci.* **2017**, *62*, 33–86. https://doi.org/10.1016/j.pecs.2017.05.004.
85. Huang, M.; Zhu, L.; Zhang, W.; et al. Insight into the synergistic reaction mechanism of biomass pseudo components and low-density polyethylene for the production of light aromatics through co-catalytic fast pyrolysis over hierarchical HZSM-5. *Fuel* **2022**, *324*, 124699. https://doi.org/10.1016/j.fuel.2022.124699.
86. Razzak, S.A.; Haddad, H.; Nawaz, A.; et al. Review for the synergistic effects in catalytic co-pyrolysis of biomass and plastic waste: Pathways to sustainable energy. *Next Sustainability* **2025**, *6*, 100157. https://doi.org/10.1016/j.nxsust.2025.100157.
87. Zhang, Y.; Wang, J.; Zhang, H.; et al. *In-situ* reaction strengthening mechanism of the pyrolysis water and bio-oil during the biomass pyrolysis over CaO and Ni-char dual catalytic system. *Energy* **2025**, *319*, 134913. https://doi.org/10.1016/j.energy.2025.134913.
88. Hasan, M.; Baheerathan, B.; Sutradhar, S.; et al. Microwave-assisted synthesis of biomass-derived N-doped carbon dots for metal ion sensing. *Carbon Res.* **2025**, *4*, 49. https://doi.org/10.1007/s44246-025-00215-7.
89. Imran, A.; Bramer, E.A.; Seshan, K.; et al. An overview of catalysts in biomass pyrolysis for production of biofuels. *Biofuel* **2018**, *5*, 872–882. https://doi.org/10.18331/BRJ2018.5.4.2.
90. Norouzi, O.; Taghavi, S.; Arku, P.; et al. What is the best catalyst for biomass pyrolysis? *J. Anal. Appl. Pyrolysis* **2021**, *158*, 105280. https://doi.org/10.1016/j.jaap.2021.105280.
91. Sun, M.H.; Chen, L.H.; Li, X.Y.; et al. A comparative study of hierarchically micro-meso-macroporous solid-acid catalysts constructed by zeolites nanocrystals synthesized via a quasi-solid-state crystallization process. *Microporous Mesoporous Mater.* **2013**, *182*, 122–135. https://doi.org/10.1016/j.micromeso.2013.08.034.
92. Mustapha, S.I.; Isa, Y.M. Co-pyrolysis of microalgae and sewage sludge over ZnO/MgO/CeO_2/HZSM-5 catalyst for energy and water treatment application. *J. Environ. Chem. Eng.* **2024**, *12*, 114955. https://doi.org/10.1016/j.jece.2024.114955.
93. Kai, W.; Xie, X.; Lin, D.; et al. Catalytic pyrolysis of paper mill sludge over self-sourced CaO/biochar catalyst under different temperatures. *Fuel* **2025**, *398*, 135538. https://doi.org/10.1016/j.fuel.2025.135538.
94. Zhou, Q.; Wu, L.; Wang, J.; et al. Catalytic fast pyrolysis of $Ca(OH)_2$-pretreated lignin over Beta zeolite for aromatic-rich bio-oil production. *Energy* **2025**, *328*, 136667. https://doi.org/10.1016/j.energy.2025.136667.
95. Rahimi, S.; Shahdadi, A.; Alizadeh, R.; et al. Conversion of polypropylene into valued-added gasoline range hydrocarbons by catalytic pyrolysis at atmospheric pressure: Different composite catalysts of HZSM-5, HY and MCM-41. *J. Taiwan Inst. Chem. Eng.* **2025**, *173*, 106184. https://doi.org/10.1016/j.jtice.2025.106184.
96. Subagyono, R.D.J.N.; Madani, N.M.; Prechisilia, C.Z.L.C.B.; et al. Pyrolysis of microalgae over Ni/Al-SBA-15 and Ni/Ga-SBA-15 catalysts prepared using a low-acidity solvent and ultrasonic-assisted sol-gel method. *J. Anal. Appl. Pyrolysis* **2025**, *186*, 106935. https://doi.org/10.1016/j.jaap.2024.106935.
97. Vichaphund, S.; Wimuktiwan, P.; Soongprasit, C.; et al. Aromatic and aliphatic production of catalytic pyrolysis of lignin using ZSM-5/Al-SBA-15 catalyst derived from high-calcium fly ash. *Energy Rep.* **2021**, *7*, 232–247. https://doi.org/10.1016/j.egyr.2021.07.127.

98. Suarez, M.A.; Santamaria, L.; Lopez, G.; et al. Oxidative steam reforming of HDPE pyrolysis volatiles on Ni catalysts: Effect of the support (Al_2O_3, ZrO_2, SiO_2) and promoter (CeO_2, La_2O_3) on the catalyst performance. *Chin. J. Catal.* **2025**, *69*, 149–162. https://doi.org/10.1016/S1872-2067(24)60222-6.
99. Ma, C.; Kamo, T. Enhanced debromination by Fe particles during the catalytic pyrolysis of non-metallic fractions of printed circuit boards over ZSM-5 and Ni/SiO_2-Al_2O_3 catalyst. *J. Anal. Appl. Pyrolysis* **2019**, *138*, 170–177. https://doi.org/10.1016/j.jaap.2018.12.021.
100. Zheng, Y.; Tao, L.; Yang, X.; et al. Comparative study on pyrolysis and catalytic pyrolysis upgrading of biomass model compounds: Thermochemical behaviors, kinetics, and aromatic hydrocarbon formation. *J. Energy Inst.* **2019**, *92*, 1348–1363. https://doi.org/10.1016/j.joei.2018.09.006.
101. Raja, N.; Monsalve-Bravo, G.M.; Kaneti, Y.V.; et al. Thermogravimetric kinetic analysis of catalytic and non-catalytic pyrolysis of simulated municipal solid waste. *Chem. Eng. J.* **2023**, *470*, 144046. https://doi.org/10.1016/j.cej.2023.144046.
102. Dammann, M.; Walker, S.C.; Mancini, M.; et al. Devolatilisation of beech wood char: Kinetics from thermogravimetric analyses and drop-tube reactor experiments. *Fuel* **2024**, *375*, 131967. https://doi.org/10.1016/j.fuel.2024.131967.
103. Alsaffar, M.A.; Mageed, A.K.; Ghany, M.A.R.A. Thermogravimetric analysis and non-isothermal kinetics of hydrocarbon-rich petroleum residues. *Sustain. Chem. Clim. Action* **2025**, *7*, 100115. https://doi.org/10.1016/j.scca.2025.100115.
104. Memon, T.A.; Ku, X.; Vasudev, V.; et al. Experimental investigation of co-pyrolysis of fruit peel waste: Impact of blending on thermal degradation behavior, kinetics, and products. *Biomass Convers. Biorefin.* **2025**, *15*, 18783–18797. https://doi.org/10.1007/s13399-025-06550-4.
105. Gamlin, C.D.; Dutta, N.K.; Choudhury, N.R.; et al. Evaluation of kinetic parameters of thermal and oxidative decomposition of base oils by conventional, isothermal and modulated TGA, and pressure DSC. *Thermochim. Acta* **2002**, *392–393*, 387–369. https://doi.org/10.1016/S0040-6031(02)00121-1.
106. Chen, T.; Liang, A.; Chen, X.; et al. Pyrolysis behavior of polypropylene and PVC medical waste: Multi-scale analysis via TGA, FTIR, GC–MS and kinetic modeling. *Therm. Sci. Eng. Prog.* **2025**, 104324. https://doi.org/10.1016/j.tsep.2025.104324.
107. Shoaib, M.; Ku, X.; Vasudev, V. Thermo-kinetic analysis of co-pyrolysis of Platanus tree leaves with coals. *Int. J. Coal Prep. Util.* **2025**, *68,* 104324. https://doi.org/10.1080/19392699.2025.2480334.
108. Vyazovkin, S.; Burnham, A.K.; Criado, J.M.; et al. ICTAC Kinetics Committee recommendations for performing kinetic computations on thermal analysis data. *Thermochim. Acta* **2011**, *520*, 1–19. https://doi.org/10.1016/j.tca.2011.03.034.
109. Vyazovkin, S.; Burnham, A.K.; Favergeon, L.; et al. ICTAC Kinetics Committee recommendations for analysis of multi-step kinetics. *Thermochim. Acta* **2020**, *689*, 178597. https://doi.org/10.1016/j.tca.2020.178597.
110. Vasudev, V.; Ku, X.; Ram, S.; et al. An Exploration of Strategies for Conducting Kinetic Analysis of Lignocellulosic and Algal Biomass Pyrolysis. *Bioenergy Res.* **2025**, *18*, 64. https://doi.org/10.1007/s12155-025-10861-9.
111. Patil, Y.; Ku, X.; Vasudev, V. Pyrolysis Characteristics and Determination of Kinetic and Thermodynamic Parameters of Raw and Torrefied Chinese Fir. *ACS Omega* **2023**, *8*, 34938–34947. https://doi.org/10.1021/acsomega.3c04328.
112. Memon, T.A.; Ku, X.; Vasudev, V. Co-Pyrolysis of Peanut Shells and Tea Plant Branches: Physicochemical Properties, Synergistic Effect and Thermo-Kinetic Analyses. *Bioenergy Res.* **2024**, *17*, 1805–1815. https://doi.org/10.1007/s12155-024-10728-5.
113. Friedman, H.L. Kinetics of thermal degradation of char-forming plastics from thermogravimetry. Application to a phenolic plastic. *J. Polym. Sci. Part C Polym. Symp.* **1964**, *6*, 183–195. https://doi.org/10.1002/polc.5070060121.
114. Balasundram, V.; Ibrahim, N.; Kasmani, R.M.; et al. Thermogravimetric catalytic pyrolysis and kinetic studies of coconut copra and rice husk for possible maximum production of pyrolysis oil. *J. Clean. Prod.* **2017**, *167*, 218–228. https://doi.org/10.1016/j.jclepro.2017.08.173.
115. Fu, W.; Zhang, Y.; Liu, Z.; et al. Kinetic and thermodynamic insights into the catalytic pyrolysis of PP with Fe/Ni catalysts. *Energy* **2025**, *330*, 136809. https://doi.org/10.1016/j.energy.2025.136809.
116. Ram, S.; Ku, X.; Vasudev, V. Catalytic pyrolysis of green algae: Influence of catalysts on thermal degradation behavior and product distribution. *Biofuels Bioprod. Biorefin.* **2025**, *19*, 1904–1914. https://doi.org/10.1002/bbb.2791.
117. Li, B.Y.; Tee, M.Y.; Nge, K.S.; et al. Comparison Kinetic Analysis between Coats-Redfern and Criado's Master Plot on Pyrolysis of Horse Manure. *Chem. Eng. Trans.* **2023**, *106*, 1273–1278. https://doi.org/10.3303/CET23106213.
118. Gözke, G. Kinetic and thermodynamic analyses based on thermogravimetric pyrolysis of watermelon seed by isoconversional and master plots methods. *Renew. Energy* **2022**, *201*, 916–927. https://doi.org/10.1016/j.renene.2022.10.100.
119. Nie, N.; Wang, Y.; Yellezuome, D.; et al. Exploring kinetic and thermodynamic mechanisms of switchgrass pyrolysis using iterative linear integral isoconversional method and master plots approach. *Fuel* **2023**, *338*, 127266. https://doi.org/10.1016/j.fuel.2022.127266.
120. Ram, S.; Vasudev, V.; Ku, X. Characterization and kinetic analysis of lignocellulosic and algal biochar combustion. *Int. J. Fluid Eng.* **2024**, *1*, 024302. https://doi.org/10.1063/5.0194358.
121. Vyazovkin, S.; Sbirrazzuoli, N. Isoconversional methods as single-step kinetic approximation. *Thermochim. Acta* **2024**, *733*, 179692. https://doi.org/10.1016/j.tca.2024.179692.

122. Vyazovkin, S. Misinterpretation of Thermodynamic Parameters Evaluated from Activation Energy and Preexponential Factor Determined in Thermal Analysis Experiments. *Thermo* **2024**, *4*, 373–381. https://doi.org/10.3390/thermo4030019.
123. Raza, A.; Khan, W.U.H.; Khoja, A.H.; et al. Thermokinetic investigation of Polyethylene Terephthalate (PET) plastic over biomass fly ash (BFA) catalyst using pyrolysis process through non-isothermal thermogravimetric analysis. *Sustain. Chem. Pharm.* **2024**, *42*, 101856. https://doi.org/10.1016/j.scp.2024.101856.
124. Rony, A.H.; Kong, L.; Lu, W.; et al. Kinetics, thermodynamics, and physical characterization of corn stover (*Zea mays*) for solar biomass pyrolysis potential analysis. *Bioresour. Technol.* **2019**, *284*, 466–473. https://doi.org/10.1016/j.biortech.2019.03.049.
125. Gotor, F.J.; Criado, J.M.; Malek, J.; et al. Kinetic analysis of solid-state reactions: The universality of master plots for analyzing isothermal and nonisothermal experiments. *J. Phys. Chem. A* **2000**, *104*, 10777–10782. https://doi.org/10.1021/jp0022205.
126. Sánchez-Jiménez, P.E.; Pérez-Maqueda, L.A.; Perejón, A.; et al. Generalized master plots as a straightforward approach for determining the kinetic model: The case of cellulose pyrolysis. *Thermochim. Acta* **2013**, *552*, 54–59. https://doi.org/10.1016/j.tca.2012.11.003.
127. Mehl, M.; Pelucchi, M.; Maffei, L.P.; et al. Developing chemical kinetic models for thermochemical applications. *Nat. Protoc.* **2025**, 135, 11100–11114. https://doi.org/10.1038/s41596-025-01195-z.
128. Polat, S.; Kılıç, Ö.F. Pyrolysis of *Chlorella vulgaris*: Kinetic analysis, advanced characterization, and bio-oil optimization. *J. Environ. Chem. Eng.* **2025**, *13*, 120374. https://doi.org/10.1016/j.jece.2025.120374.
129. Shen, T.; Wu, T.; Liang, Y.; et al. Kinetic analysis and neural network-based prediction of TGA curves during the co-pyrolysis of industrial hemp waste and polyvinyl chloride. *J. Anal. Appl. Pyrolysis* **2026**, *193*, 107463. https://doi.org/10.1016/j.jaap.2025.107463.
130. Petrovič, A.; Vohl, S.; Gruber, S.; et al. Thermogravimetric, kinetic and thermodynamic behaviour of raw and hydrothermally pretreated oil cakes during pyrolysis and TG-FTIR analysis of the gaseous products. *Renew. Energy* **2025**, *247*, 123041. https://doi.org/10.1016/j.renene.2025.123041.
131. Liu, Y.; Jiang; Huang, Z. Comprehensive pyrolysis study and kinetic analysis of PMMA/H-β zeolite hybrids using the Gaussian deconvolution method. *Therm. Sci. Eng. Prog.* **2025**, *62*, 103563. https://doi.org/10.1016/j.tsep.2025.103563.
132. Liu, M.; Tao, J.; Mu, L.; et al. Machine learning-driven predictions of biochar yield and NPK composition: Insights into biomass pyrolysis with data augmentation and model interpretability. *Carbon Res.* **2025**, *4*, 62. https://doi.org/10.1007/s44246-025-00229-1.
133. Xiao, K.; Zhu, X. Machine Learning Approach for the Prediction of Biomass Waste Pyrolysis Kinetics from Preliminary Analysis. *ACS Omega* **2024**, *9*, 48125–48136. https://doi.org/10.1021/acsomega.4c04649.
134. Zhang, J.; Liu, J.; Evrendilek, F.; et al. TG-FTIR and Py-GC/MS analyses of pyrolysis behaviors and products of cattle manure in CO_2 and N_2 atmospheres: Kinetic, thermodynamic, and machine-learning models. *Energy Convers. Manag.* **2019**, *195*, 346–359. https://doi.org/10.1016/j.enconman.2019.05.019.
135. Potnuri, R.; Suriapparao, D.V.; Rao, C.S.; et al. Effect of dry torrefaction pretreatment of the microwave-assisted catalytic pyrolysis of biomass using the machine learning approach. *Renew. Energy* **2022**, *197*, 798–809. https://doi.org/10.1016/j.renene.2022.08.006.
136. Akbari, A.; Sokhansanj, A.; Shfiee, M.; et al. Structural and adsorptive comparison of activated hydrochar and biochar: Machine learning analysis and novel driven kinetic and thermodynamic insight. *J. Water Process Eng.* **2025**, *76*, 108164. https://doi.org/10.1016/j.jwpe.2025.108164.
137. Li, J.; Liu, T.; Palansooriya, K.N.; et al. Zeolite-catalytic pyrolysis of waste plastics: Machine learning prediction, interpretation, and optimization. *Appl. Energy* **2025**, *382*, 125258. https://doi.org/10.1016/j.apenergy.2024.125258.
138. Mahanta, B.K.; Kumar, S.; Pathak, S.K.; et al. Machine learning-based prediction of high-entropy alloys for hydrogen storage with optimized thermodynamic and kinetic parameters. *J. Energy Storage* **2025**, *139*, 118865. https://doi.org/10.1016/j.est.2025.118865.
139. Hazmi, B.; Farooq, H.; Rashid, U.; et al. Characterization and pyrolysis kinetic modelling of lignocellulosic waste from rambutan seeds: A machine learning approach. *Biomass Bioenergy* **2026**, *204*, 108426. https://doi.org/10.1016/j.biombioe.2025.108426.
140. Tagade, A.; Kandpal, S.; Singh, S.; et al. Kinetic and thermodynamic analyses of pyrolysis of finger millet (*Eleusine coracana*) straw through both model-free and model-based methods and application of ANN-based machine learning model to predict thermal degradation. *Bioresour. Technol. Rep.* **2025**, *30*, 102139. https://doi.org/10.1016/j.biteb.2025.102139.
141. Wang, S.; Shi, Z.; Jin, Y.; et al. A machine learning model to predict the pyrolytic kinetics of different types of feedstocks. *Energy Convers. Manag.* **2022**, *260*, 115613. https://doi.org/10.1016/j.enconman.2022.115613.
142. Khandelwal, K.; Nanda, S.; Dalai, A.K. Machine learning to predict the production of bio-oil, biogas, and biochar by pyrolysis of biomass: A review. *Environ. Chem. Lett.* **2024**, *22*, 2669–2698. https://doi.org/10.1007/s10311-024-01767-7.

143. Cardarelli, A.; Ciambella, M.; Fornai, P.; et al. Kinetic analysis and prediction modeling by advanced machine learning of pyrolysis of dairy cattle manure from conventional and organic systems. *Biomass Bioenergy* **2025**, *202*, 108247. https://doi.org/10.1016/j.biombioe.2025.108247.
144. Tiwari, A.; Rao, C.S.; Jammula, K.; et al. Kinetic analysis and machine learning insights in the production of biochar from *Artocarpus heterophyllus* (jackfruit) through pyrolysis. *Biomass Bioenergy* **2025**, *201*, 108125. https://doi.org/10.1016/j.biombioe.2025.108125.
145. Zhong, Y.; Liu, F.; Huang, G.; et al. Thermogravimetric experiments based prediction of biomass pyrolysis behavior: A comparison of typical machine learning regression models in Scikit-learn. *Mar. Pollut. Bull.* **2024**, *202*, 116361. https://doi.org/10.1016/j.marpolbul.2024.116361.
146. Gao, W.; Zhang, Y.; Wang, Y.; et al. Pyrolysis characteristics and kinetic analysis of coating pitch derived from ethylene tar using model-free and model-fitting methods. *J. Anal. Appl. Pyrolysis* **2024**, *183*, 106803. https://doi.org/10.1016/j.jaap.2024.106803.
147. Bharti, B.; Kandpal, S.; Sawarkar, A.N.; et al. Holistic approach for sequential transesterification and pyrolysis of microalgal biomass: Kinetic and thermodynamic analysis of pyrolysis using model-free and model-based approaches. *Renew. Energy* **2024**, *235*, 121319. https://doi.org/10.1016/j.renene.2024.121319.
148. Sbirrazzuoli, N. Kinetic analysis of complex chemical reactions by coupling model-free and model-fitting analysis. *Thermochim. Acta* **2023**, *719*, 179416. https://doi.org/10.1016/j.tca.2022.179416.
149. Budrugeac, P. On the use of the model-free way method for kinetic analysis of thermoanalytical data—Advantages and limitations. *Thermochim. Acta* **2021**, *706*, 179063. https://doi.org/10.1016/j.tca.2021.179063.
150. Aggarwal, N.; Pham, H.L.; Ranjan, B.; et al. Microbial engineering strategies to utilize waste feedstock for sustainable bioproduction. *Nat. Rev. Bioeng.* **2024**, *2*, 155–174. https://doi.org/10.1038/s44222-023-00129-2.
151. Mastry, M.C.; Dorazio, L.; Fu, J.C.; et al. Processing renewable and waste-based feedstocks with fluid catalytic cracking: Impact on catalytic performance and considerations for improved catalyst design. *Front. Chem.* **2023**, *11*, 1067488. https://doi.org/10.3389/fchem.2023.1067488.
152. Ullah, K.; Sharma, V.K.; Ahmad, M.; et al. The insight views of advanced technologies and its application in bio-origin fuel synthesis from lignocellulose biomasses waste, a review. *Renew. Sustain. Energy Rev.* **2018**, *82*, 3992–4008. https://doi.org/10.1016/j.rser.2017.10.074.
153. Kumar, R.; Strezov, V.; Weldekidan, H.; et al. Lignocellulose biomass pyrolysis for bio-oil production: A review of biomass pre-treatment methods for production of drop-in fuels. *Renew. Sustain. Energy Rev.* **2020**, *123*, 109763. https://doi.org/10.1016/j.rser.2020.109763.
154. Escalante, J.; Chen, W.H.; Tabatabaei, M.; et al. Pyrolysis of lignocellulosic, algal, plastic, and other biomass wastes for biofuel production and circular bioeconomy: A review of thermogravimetric analysis (TGA) approach. *Renew. Sustain. Energy Rev.* **2022**, *169*, 112914. https://doi.org/10.1016/j.rser.2022.112914.
155. Vassilev, S.V.; Vassileva, C.G. Composition, properties and challenges of algae biomass for biofuel application: An overview. *Fuel* **2016**, *181*, 1–33. https://doi.org/10.1016/j.fuel.2016.04.106.
156. Kumar, M.; Sun, Y.; Rathour, R.; et al. Algae as potential feedstock for the production of biofuels and value-added products: Opportunities and challenges. *Sci. Total Environ.* **2020**, *716*, 137116. https://doi.org/10.1016/j.scitotenv.2020.137116.
157. Rebrov, E.; Panjabi, R.; Mong, G.R.; et al. Reaction kinetics and product distributions in thermal and catalytic pyrolysis of agricultural mulch films over HZSM-5 zeolite. *Chem. Eng. J.* **2025**, *522*, 167458. https://doi.org/10.1016/j.cej.2025.167458.
158. Wang, S.; Lin, H.; Ru, B.; et al. Kinetic modeling of biomass components pyrolysis using a sequential and coupling method. *Fuel* **2016**, *185*, 763–771. https://doi.org/10.1016/j.fuel.2016.08.037.
159. Wang, C.; Li, L.; Zeng, Z.; et al. Catalytic performance of potassium in lignocellulosic biomass pyrolysis based on an optimized three-parallel distributed activation energy model. *Bioresour. Technol.* **2019**, *281*, 412–420. https://doi.org/10.1016/j.biortech.2019.02.118.
160. Kavade, O.G.; Dhepe, P.L.; Devi, N.R.; et al. Experimental investigation and lumped kinetic modeling studies for upcycling of polyolefins. *J. Indian Chem. Soc.* **2025**, *102*, 102127. https://doi.org/10.1016/j.jics.2025.102127.
161. Suleiman, M.Y.; Benedetto, E.; Piazza, V.; et al. Kinetic modelling of biomass pyrolysis: A new lumped scheme for xylan-based hardwood hemicellulose. *Energy Convers. Manag. X* **2025**, *27*, 101130. https://doi.org/10.1016/j.ecmx.2025.101130.
162. Tanha, M.A.; Kazemeini, M.; Hosseinpour, V.; et al. A genetic algorithm aimed at developing a lumped kinetic model for conversion of ethyl mercaptan into hydrogen sulfide on an H-ZSM-5 catalyst. *Results Eng.* **2025**, *27*, 105784. https://doi.org/10.1016/j.rineng.2025.105784.
163. Bach, Q.V.; Chen, W.H. Pyrolysis characteristics and kinetics of microalgae via thermogravimetric analysis (TGA): A state-of-the-art review. *Bioresour. Technol.* **2017**, *246*, 88–100. https://doi.org/10.1016/j.biortech.2017.06.087.
164. Wang, W.; Li, Y.; Li, Y.; et al. Activation energy calculation method for waste plastic pyrolysis based on a difference-weighted model. *Fuel* **2026**, *405*, 136754. https://doi.org/10.1016/j.fuel.2025.136754.

165. He, X.C.; Chen, D.Z. ReaxFF MD study on the early stage co-pyrolysis of mixed PE/PP/PS plastic waste. *J. Fuel Chem. Technol.* **2022**, *50*, 346–356. https://doi.org/10.1016/S1872-5813(21)60161-5.
166. Handawy, M.K.M.; Abdellatief, T.M.M.; Duan, X.; et al. A hybrid AI-kinetic framework for predicting the pyrolysis of food packaging plastic waste: Integrating TGA, model-free kinetics, and artificial neural networks. *Appl. Energy Combust. Sci.* **2025**, *24*, 100418. https://doi.org/10.1016/j.jaecs.2025.100418.
167. Riaz, S.; Ahmad, N.; Farooq, W; et al. Catalytic pyrolysis of HDPE for enhanced hydrocarbon yield: A boosted regression tree assisted kinetics study for effective recycling of waste plastic. *Digit. Chem. Eng.* **2025**, *14*, 100213. https://doi.org/10.1016/j.dche.2024.100213.
168. Martínez-Narro, G.; Royston, N.J.; Billsborough, K.L.; et al. Kinetic modelling of mixed plastic waste pyrolysis. *Chem. Thermodyn. Therm. Anal.* **2023**, *9*, 100105. https://doi.org/10.1016/j.ctta.2023.100105.
169. Armenise, S.; Luing, W.S.; Vázquez, M.A.R.; et al. Tailoring catalyst acidity and hierarchical pore structure for enhanced BTX yields in plastic waste pyrolysis. *J. Environ. Chem. Eng.* **2025**, *13*, 119493. https://doi.org/10.1016/j.jece.2025.119493.
170. Das, P. Pyrolysis study of a waste plastic mixture through different kinetic models using isothermal and nonisothermal mechanism. *RSC Adv.* **2024**, *14*, 25599–25618. https://doi.org/10.1039/d4ra04957h.
171. Pyo, S.; Kim, Y.M.; Park, Y.; et al. Catalytic pyrolysis of polypropylene over Ga loaded HZSM-5. *J. Ind. Eng. Chem.* **2021**, *103*, 136–141. https://doi.org/10.1016/j.jiec.2021.07.027.
172. Majidian, N.; Saleh, M.; Samipourgiri, M. Kinetics study of catalytic pyrolysis of polystyrene polymer using response surface method. *Iran. Polym. J.* **2024**, *33*, 1793–1806. https://doi.org/10.1007/s13726-024-01362-1.
173. Li, M.; Jia, Y.; Chen, D.; et al. Exploring pyrolysis mechanism of waste PET in different degrees of polymerization to regulate the pyrolysis products. *Polym. Degrad. Stab.* **2025**, *233*, 111175. https://doi.org/10.1016/j.polymdegradstab.2025.111175.
174. Miskolczi, N.; Gao, N.B.; Quan, C. Transformation of biomass and waste plastic mixtures into hydrocarbon oils and gases by pyrolysis using different reactor temperatures and pressures. *J. Anal. Appl. Pyrolysis* **2024**, *180*, 106520. https://doi.org/10.1016/j.jaap.2024.106520.
175. Chen, G.; Cao, X.; Che, Y.; et al. Synergistic effect on low-pressure pyrolysis of biomass-plastic mixture as representative of Tibetan tourism solid waste. *J. Anal. Appl. Pyrolysis* **2023**, *175*, 106181. https://doi.org/10.1016/j.jaap.2023.106181.
176. Wu, Z.; Li, Y.; Zhang, B.; et al. Co-pyrolysis behavior of microalgae biomass and low-rank coal: Kinetic analysis of the main volatile products. *Bioresour. Technol.* **2019**, *271*, 202–209. https://doi.org/10.1016/j.biortech.2018.09.076.
177. Cui, Q.; Ma, X.; Nakano, K.; et al. Effect of blending on hydrotreating reactivities of atmospheric residues: Synergistic effects. *Fuel* **2021**, *293*, 120429. https://doi.org/10.1016/j.fuel.2021.120429.
178. Vo, T.A.; Tran, Q.K.; Ly, H.V.; et al. Co-pyrolysis of lignocellulosic biomass and plastics: A comprehensive study on pyrolysis kinetics and characteristics. *J. Anal. Appl. Pyrolysis* **2022**, *163*, 105464. https://doi.org/10.1016/j.jaap.2022.105464.
179. Xu, G.; Yang, X.; Zhang, J.; et al. Nitrogen-sulfur transport, products, and synergistic effects in the co-pyrolysis of the CaO/K_2FeO_4 conditioned sludge and chlorella. *J. Energy Inst.* **2025**, *125*, 102421. https://doi.org/10.1016/j.joei.2025.102421.
180. Li, Y.; Guo, Z.; Zhu, H.; et al. Thermal behavior and K–Fe synergistic effects in the catalytic pyrolysis of Chinese herb residues for H_2-rich syngas. *Int. J. Hydrogen Energy* **2025**, *196*, 152543. https://doi.org/10.1016/j.ijhydene.2025.152543.
181. Xu, S.; Cao, B.; Uzoejinwa, B.B.; et al. Synergistic effects of catalytic co-pyrolysis of macroalgae with waste plastics. *Process Saf. Environ. Prot.* **2020**, *137*, 34–48. https://doi.org/10.1016/j.psep.2020.02.001.
182. Dussan, K.; Dooley, S.; Monaghan, R.F.D.; et al. New Pseudo-Components of Hemicellulose and Lignin. In Proceedings of the 25th European Biomass Conference and Exhibition, Stockholm, Sweden 12–15 June2017; pp. 971–979. https://doi.org/10.5071/25thEUBCE2017-3BO.11.3.
183. Sipra, A.T.; Gao, N.; Sarwar, H. Municipal solid waste (MSW) pyrolysis for bio-fuel production: A review of effects of MSW components and catalysts. *Fuel Process. Technol.* **2018**, *175*, 131–147. https://doi.org/10.1016/j.fuproc.2018.02.012.
184. Sawatmongkhon, B.; Promhuad, P.; Wongkhorsub, C.; et al. Kinetic analysis of diesel particulate matter oxidation using a multi-step reaction model, components peak deconvolution, and isoconversional methods. *Fuel* **2025**, *390*, 134644. https://doi.org/10.1016/j.fuel.2025.134644.
185. Kumar, A. Co-pyrolysis of microalgae residue and sewage sludge: An in-depth characterization of kinetics, drivers, and gas-oil-char behaviors. *J. Anal. Appl. Pyrolysis* **2024**, *179*, 106438. https://doi.org/10.1016/j.jaap.2024.106438.
186. Adhikari, R.; Rabinovitch, J.; Parziale, N.; et al. Hierarchical kinetic analysis for development of a reduced-order model of the multi-step thermal decomposition of munitions wastewater. *Thermochim. Acta* **2025**, *750*, 180038. https://doi.org/10.1016/j.tca.2025.180038.
187. Locaspi, A.; Faravelli, T. Generalized derivation of multi-step kinetic models for polymer condensed-phase pyrolysis: Application to poly(ethylene terephthalate). *Proc. Combust. Inst.* **2025**, *41*, 105978. https://doi.org/10.1016/j.proci.2025.105978.
188. Liu, C.; Zhang, B.; Bian, Y.; et al. Synergistic effect and kinetic analysis of catalytic co-pyrolysis of waste cotton swabs and non-woven masks. *J. Anal. Appl. Pyrolysis* **2022**, *167*, 105677. https://doi.org/10.1016/j.jaap.2022.105677.

189. Wang, S.; Wu, K.; Yu, J.; et al. Kinetic and thermodynamic analysis of biomass catalytic pyrolysis with nascent biochar in a two-stage reactor. *Combust. Flame* **2023**, *251*, 112671. https://doi.org/10.1016/j.combustflame.2023.112671.
190. Zheng, Y.; Li, D.; Pei, T.; et al. Mechanism of synergistic effects and kinetic analysis in bamboo-LDPE waste ex-situ catalytic co-pyrolysis for enhanced aromatic hydrocarbon production via CeZrAl and HZSM-5 dual catalyst. *J. Environ. Chem. Eng.* **2022**, *10*, 107479. https://doi.org/10.1016/j.jece.2022.107479.
191. Okonsky, S.T.; Krishna, J.V.J.; Lee, D.H.; et al. Kinetic modelling and measurement of catalyst deactivation for the catalytic co-pyrolysis of PP and PET with HZSM-5. *Appl. Catal. A Gen.* **2025**, *708*, 120574. https://doi.org/10.1016/j.apcata.2025.120574.
192. Huang, S.; Su, Y.; Luo, W.; et al. Kinetic analysis and in-situ no support catalytic pyrolysis product distribution of Chinese herb residue. *J. Anal. Appl. Pyrolysis* **2021**, *156*, 105114. https://doi.org/10.1016/j.jaap.2021.105114.
193. Fong, M.J.B.; Loy, A.C.M.; Chin, B.L.F.; et al. Catalytic pyrolysis of *Chlorella vulgaris*: Kinetic and thermodynamic analysis. *Bioresour. Technol.* **2019**, *289*, 121689. https://doi.org/10.1016/j.biortech.2019.121689.
194. Panicker, T.F.; Gupta, R.; Mishra, R.K.; et al. Thermo-catalytic pyrolysis and kinetic study of non-edible castor seeds into renewable liquid fuel and value-added chemicals. *Energy Rep.* **2025**, *14*, 2280–2295. https://doi.org/10.1016/j.egyr.2025.08.050.
195. Yang, J.; Xu, X.; Liang, S.; et al. Enhanced hydrogen production in catalytic pyrolysis of sewage sludge by red mud: Thermogravimetric kinetic analysis and pyrolysis characteristics. *Int. J. Hydrogen Energy* **2018**, *43*, 7795–7807. https://doi.org/10.1016/j.ijhydene.2018.03.018.
196. Dwivedi, P.; Rathore, A.K. Thermogravimetric kinetic study of catalytic and non-catalytic pyrolysis of PET bottles and micro carbon rod formation. *J. Chem. Thermodyn.* **2025**, *209*, 107530. https://doi.org/10.1016/j.jct.2025.107530.
197. Sharma, H.; Chakinala, N.; Thota, C.; et al. Exploring the catalytic conversion of pyrolytic wax residue: Kinetics and co-pyrolysis. *J. Anal. Appl. Pyrolysis* **2026**, *193*, 107331. https://doi.org/10.1016/j.jaap.2025.107331.
198. Kumar, R.; Manoth, A.; Mondal, M.K. Pyrolysis behavior of native and Ni-Fe treated biomass: Kinetic modeling and thermodynamic insights. *Therm. Sci. Eng. Prog.* **2025**, *66*, 104026. https://doi.org/10.1016/j.tsep.2025.104026.
199. Farooq, W.; Ali, I.; Naqvi, S.R.; et al. Evolved Gas Analysis and Kinetics of Catalytic and Non-Catalytic Pyrolysis of Microalgae *Chlorella* sp. Biomass with Ni/θ-Al_2O_3 Catalyst via Thermogravimetric Analysis. *Front. Energy Res.* **2021**, *9*, 775037. https://doi.org/10.3389/fenrg.2021.775037.
200. Eimontas, J.; Yousef, S.; Striūgas, N.; et al. Catalytic pyrolysis kinetic behaviour and TG-FTIR-GC–MS analysis of waste fishing nets over ZSM-5 zeolite catalyst for caprolactam recovery. *Renew. Energy* **2021**, *179*, 1385–1403. https://doi.org/10.1016/j.renene.2021.07.143.
201. Wang, P.; Shen, Y. Catalytic pyrolysis of cellulose and chitin with calcined dolomite—Pyrolysis kinetics and products analysis. *Fuel* **2022**, *312*, 122875. https://doi.org/10.1016/j.fuel.2021.122875.
202. Yu, L.; Shi, X.; Zhang, S.; et al. A comprehensive investigation of kinetic and thermodynamic analysis to catalytic pyrolysis bamboo with N-doped biochar. *Fuel* **2025**, *396*, 135312. https://doi.org/10.1016/j.fuel.2025.135312.
203. Oliveira, C.C.; dos Santos, G.E.S.; Vieira, L.G.M.; et al. Catalytic Co-pyrolysis of soybean husk and high-density polyethylene: Artificial neural network modeling and synergistic approach for enhanced gasoline-range biofuel production using zeolite HZSM-5. *Renew. Energy* **2026**, *256*, 124148. https://doi.org/10.1016/j.renene.2025.124148.
204. Hassan, H.; Hameed, B.H.; Lim, J.K. Co-pyrolysis of sugarcane bagasse and waste high-density polyethylene: Synergistic effect and product distributions. *Energy* **2020**, *191*, 116545. https://doi.org/10.1016/j.energy.2019.116545.
205. Nardella, F.; Bellavia, S.; Mattonai, M.; et al. Co-pyrolysis of biomass and plastic: Synergistic effects and estimation of elemental composition of pyrolysis oil by analytical pyrolysis–gas chromatography/mass spectrometry. *Bioresour. Technol.* **2022**, *354*, 127170. https://doi.org/10.1016/j.biortech.2022.127170.
206. Özsin, G.; Pütün, A.E. TGA/MS/FT-IR study for kinetic evaluation and evolved gas analysis of a biomass/PVC co-pyrolysis process. *Energy Convers. Manag.* **2019**, *182*, 143–153. https://doi.org/10.1016/j.enconman.2018.12.060.
207. Nawaz, A.; Razzak, S.A. Synergism, pyrolysis performance, product distribution and characteristics in the co-pyrolysis of date palm waste and polyethylene foam: Harnessing the potential of plastics and biomass valorization. *Carbon Resour. Convers.* **2025**, *8*, 100312. https://doi.org/10.1016/j.crcon.2025.100312.
208. Yang, C.; Li, C.; Liu, H.; et al. Co-pyrolysis of waste office paper and high-density polyethylene: Product distribution, kinetics and reaction mechanism. *J. Energy Inst.* **2025**, *120*, 102105. https://doi.org/10.1016/j.joei.2025.102105.
209. Fu, J.; Wu, X.; Liu, J.; et al. Co-circularity of spent coffee grounds and polyethylene via co-pyrolysis: Characteristics, kinetics, and products. *Fuel* **2023**, *337*, 127061. https://doi.org/10.1016/j.fuel.2022.127061.
210. Jae, J.; Tompsett, G.A.; Foster, A.J.; et al. Investigation into the shape selectivity of zeolite catalysts for biomass conversion. *J. Catal.* **2011**, *279*, 257–268. https://doi.org/10.1016/j.jcat.2011.01.019.
211. French, R.; Czernik, S. Catalytic pyrolysis of biomass for biofuels production. *Fuel Process. Technol.* **2010**, *91*, 25–32. https://doi.org/10.1016/j.fuproc.2009.08.011.

212. Carlson, T.R.; Cheng, Y.T.; Jae, J.; et al. Production of green aromatics and olefins by catalytic fast pyrolysis of wood sawdust. *Energy Environ. Sci.* **2011**, *4*, 145–161. https://doi.org/10.1039/c0ee00341g.
213. Ochoa, A.; Bilbao, J.; Gayubo, A.G.; et al. Coke formation and deactivation during catalytic reforming of biomass and waste pyrolysis products: A review. *Renew. Sustain. Energy Rev.* **2020**, *119*, 109600. https://doi.org/10.1016/j.rser.2019.109600.
214. Ranzi, E.; Debiagi, P.E.A.; Frassoldati, A. Mathematical Modeling of Fast Biomass Pyrolysis and Bio-Oil Formation. Note II: Secondary Gas-Phase Reactions and Bio-Oil Formation. *ACS Sustainable Chem. Eng.* **2017**, *5*, 2882–2896. https://doi.org/10.1021/acssuschemeng.6b03098.
215. Kanchan, D.R.; Banerjee, A. Role of support in phenol hydrodeoxygenation over supported Pd catalysts: Insights from first-principles based microkinetic modelling. *J. Catal.* **2025**, *450*, 116266. https://doi.org/10.1016/j.jcat.2025.116266.
216. Gracia, A.; Lozano-Reis, P.; Huarte-Larrañaga, F.; et al. CO_2 hydrogenation on Ni(111): Microkinetic modelling vs. kinetic Monte Carlo simulations—Choosing the right approach for unravelling reaction kinetics. *RSC Sustain.* **2025**, *3*, 3499–3512. https://doi.org/10.1039/d5su00240k.
217. Liu, D.; Bai, Y.; Chen, D.; et al. Catalytic pyrolysis of n-paraffin coexisting with olefin over ZSM-5 based catalysts: Experiments, kinetics, and DFT calculations. *Chem. Eng. Sci.* **2026**, *320*, 122533. https://doi.org/10.1016/j.ces.2025.122533.
218. Chen, D.; Liu, D.; He, H.; et al. Rational tuning of monomolecular, bimolecular and aromatization pathways in the catalytic pyrolysis of hexane on ZSM-5 from a first-principles-based microkinetics analysis. *Fuel* **2024**, *366*, 131368. https://doi.org/10.1016/j.fuel.2024.131368.
219. Chen, D.; Wang, H.; Wei, J.; et al. Reaction mechanism and microkinetics of 1-hexene catalytic pyrolysis on HZSM-5: A first-principles study. *Chem. Eng. Sci.* **2023**, *282*, 119220. https://doi.org/10.1016/j.ces.2023.119220.
220. Ugwu, L.I.; Morgan, Y.; Ibrahim, H. Application of density functional theory and machine learning in heterogenous-based catalytic reactions for hydrogen production. *Int. J. Hydrogen Energy* **2022**, *47*, 2245–2267. https://doi.org/10.1016/j.ijhydene.2021.10.208.
221. Wang, Y.; Yao, Z.; Deng, S.; et al. Unravelling the reaction mechanism for the AP decomposition over MgO: A density functional theory study and microkinetic simulation. *Mater. Today Commun.* **2024**, *39*, 108658. https://doi.org/10.1016/j.mtcomm.2024.108658.
222. Luo, H.; Wang, X.; Krochmalny, K.; et al. Assessments and analysis of lumped and detailed pyrolysis kinetics for biomass torrefaction with particle-scale modeling. *Biomass Bioenergy* **2022**, *166*, 106619. https://doi.org/10.1016/j.biombioe.2022.106619.
223. Rodríguez, S.; Trueba, D.; Escribano, M.; et al. Six-lump kinetic model for plastic pyrolysis oil (PPO) and vacuum gasoil (VGO) blend hydroprocessing considering selective catalyst deactivation. *Catal. Today* **2025**, *457*, 115341. https://doi.org/10.1016/j.cattod.2025.115341.
224. Bjelić, A.; Garbarino, L.I.; Grilc, M.; et al. Continuous lumping modelling of reductive lignin depolymerization kinetics in the presence of a Ru/C catalyst. *Chem. Eng. Sci.* **2025**, *317*, 122096. https://doi.org/10.1016/j.ces.2025.122096.
225. Vicente, H.; Aguayo, A.T.; Castaño, P.; et al. Dual-cycle-based lumped kinetic model for methanol-to-aromatics (MTA) reaction over H-ZSM-5 zeolites of different Si/Al ratio. *Fuel* **2024**, *361*, 130704. https://doi.org/10.1016/j.fuel.2023.130704.
226. Jaroenkhasemmeesuk, C.; Tippayawong, N.; Shimpalee, S.; et al. Improved simulation of lignocellulosic biomass pyrolysis plant using chemical kinetics in Aspen Plus® and comparison with experiments. *Alexandria Eng. J.* **2023**, *63*, 199–209. https://doi.org/10.1016/j.aej.2022.07.060.
227. Khongprom, P.; Ratchasombat, S.; Wanchan, W.; et al. Scaling of catalytic cracking fluidized bed downer reactor based on CFD simulations—Part II: Effect of reactor scale. *RSC Adv.* **2022**, *12*, 21394–21405. https://doi.org/10.1039/d2ra03448d.
228. Ciesielski, P.N.; Pecha, M.B.; Thornburg, N.E.; et al. Bridging Scales in Bioenergy and Catalysis: A Review of Mesoscale Modeling Applications, Methods, and Future Directions. *Energy Fuels* **2021**, *35*, 14382–14400. https://doi.org/10.1021/acs.energyfuels.1c02163.
229. Mutlu, Ö.Ç.; Zeng, T. Challenges and Opportunities of Modeling Biomass Gasification in Aspen Plus: A Review. *Chem. Eng. Technol.* **2020**, *43*, 1674–1689. https://doi.org/10.1002/ceat.202000068.
230. Micale, D.; Uglietti, R.; Bracconi, M.; et al. Coupling euler-euler and microkinetic modeling for the simulation of fluidized bed reactors: An application to the oxidative coupling of methane. *Ind. Eng. Chem. Res.* **2021**, *60*, 6687–6697. https://doi.org/10.1021/acs.iecr.0c05845.
231. Nestler, F.; Müller, V.P.; Ouda, M.; et al. A novel approach for kinetic measurements in exothermic fixed bed reactors: Advancements in non-isothermal bed conditions demonstrated for methanol synthesis. *React. Chem. Eng.* **2021**, *6*, 1092–1107. https://doi.org/10.1039/d1re00071c.
232. Cheah, Y.W.; Salam, M.A.; Sebastian, J.; et al. Upgrading of triglycerides, pyrolysis oil, and lignin over metal sulfide catalysts: A review on the reaction mechanism, kinetics, and catalyst deactivation. *J. Environ. Chem. Eng.* **2023**, *11*, 109614. https://doi.org/10.1016/j.jece.2023.109614.

233. Jiang, W.; Ma, X.; Zhang, D.; et al. Highly efficient catalysts for hydrogen generation through methanol steam reforming: A critical analysis of modification strategies, deactivation, mechanisms and kinetics. *J. Ind. Eng. Chem.* **2024**, *130*, 54–72. https://doi.org/10.1016/j.jiec.2023.09.043.
234. Vares, M.; Sari, A.; Yaripour, F. Intrinsic reaction and deactivation kinetics of Methanol-to-Propylene process (MTP) over an industrial ZSM-5 catalyst. *Fuel* **2025**, *383*, 133861. https://doi.org/10.1016/j.fuel.2024.133861.
235. Muhammad, I.; Makwashi, N.; Ahmed, T.G.; et al. A Mechanistic Model on Catalyst Deactivation by Coke Formation in a CSTR Reactor. *Processes* **2023**, *11*, 944. https://doi.org/10.3390/pr11030944.
236. Noor, E.; Flamholz, A.; Liebermeister, W.; et al. A note on the kinetics of enzyme action: A decomposition that highlights thermodynamic effects. *FEBS Lett.* **2013**, *587*, 2772–2777. https://doi.org/10.1016/j.febslet.2013.07.028.
237. Chaouati, N.; Soualah, A.; Pinard, L. Coke toxicities, descriptors of the deactivating effect of coke on microporous and desilicated mordenite zeolite. *React. Kinet. Mech. Catal.* **2023**, *136*, 2243–2257. https://doi.org/10.1007/s11144-023-02447-3.
238. Langer, M.; Waldner, M.; Freund, H. Modeling of the combined deactivation and reaction kinetic behavior of an impregnated Ni/Al_2O_3 catalyst in the CO_2 methanation reaction. *Chem. Eng. J.* **2025**, *524*, 169363. https://doi.org/10.1016/j.cej.2025.169363.
239. Wei, H.L.; Jihou, Z.Q.; Liu, X.Q.; et al. Long-term alkaline deactivation of Cu-based catalyst in formaldehyde ethynylation: Mechanism and kinetic analysis. *Chem. Eng. J.* **2025**, *525*, 170651. https://doi.org/10.1016/j.cej.2025.170651.
240. Deng, Z.H.; Shi, R.; Ren, L.; et al. Catalyst deactivation model involving autocatalytic effect for the residue hydrotreating process. *Pet. Sci.* **2025**, *22*, 3447–3460. https://doi.org/10.1016/j.petsci.2025.04.031.
241. Khatri, I.; Garg, A. Use of heterogeneous activated carbon supported copper catalyst for catalytic wet oxidation of biomethanated spent wash: Reaction kinetics, catalyst stability, catalyst deactivation kinetics and biochemical methane potential. *J. Water Process Eng.* **2021**, *44*, 102387. https://doi.org/10.1016/j.jwpe.2021.102387.
242. Nicola, B.P.; Giner, E.A.; Romay, M.; et al. Challenging the deactivation resistance of Co/Cu-dendritic ZSM-5 zeolites in methane pyrolysis for clean hydrogen. *Microporous Mesoporous Mater.* **2025**, *401*, 113939. https://doi.org/10.1016/j.micromeso.2025.113939.
243. Gromotka, Z.; Yablonsky, G.; Ostrovskii, N.; et al. Integral Characteristic of Complex Catalytic Reaction Accompanied by Deactivation. *Catalysts* **2022**, *12*, 1283. https://doi.org/10.3390/catal12101283.